Self-consistent description of multipole strength in exotic nuclei: Method

J. Terasaki,[1,2,3,4,*] J. Engel,[1,†] M. Bender,[5,‡] J. Dobaczewski,[2,3,4,6,§]
W. Nazarewicz,[2,3,6,ᶜ] and M. Stoitsov[2,3,4,7,**]

[1]*Department of Physics and Astronomy, CB3255,*
University of North Carolina, Chapel Hill, North Carolina 27599-3255
[2]*Department of Physics and Astronomy,*
University of Tennessee, Knoxville, Tennessee 37996
[3]*Physics Division, Oak Ridge National Laboratory,*
Post Office Box 2008, Oak Ridge, Tennessee 37831
[4]*Joint Institute for Heavy-Ion Research, Oak Ridge, Tennessee 37831*
[5]*Physics Division, Argonne National Laboratory, Argonne, Illinois 60439*
[6]*Institute of Theoretical Physics, Warsaw University,*
ul. Hoża 69, 00-681 Warsaw, Poland
[7]*Institute of Nuclear Research and Nuclear Energy,*
Bulgarian Academy of Science, Sofia 1784, Bulgaria

We use the canonical Hartree-Fock-Bogoliubov basis to implement a self-consistent quasiparticle-random-phase approximation (QRPA) with arbitrary Skyrme energy density functionals and density-dependent pairing functionals. The point of the approach is to accurately describe multipole strength functions in spherical even-even nuclei, including weakly bound drip-line systems. We describe the method and carefully test its accuracy, particularly in handling spurious modes. To illustrate our approach, we calculate isoscalar and isovector monopole, dipole, and quadrupole strength functions in several Sn isotopes, both in the stable region and at the drip lines. We also investigate the consequences of neglecting the spin-orbit or Coulomb residual interactions in the QRPA.

I. INTRODUCTION

The study of nuclei far from stability is an increasingly important part of nuclear physics [1,2]. As radioactive beams allow more experiments on these nuclei, theoretical modeling is changing in significant ways. New ideas and progress in computer technology have allowed nuclear theorists to understand bits and pieces of nuclear structure quantitatively [3]. Short-lived exotic nuclei offer unique tests of those aspects of our developing many-body theories that depend on neutron excess [4]. The major challenge is to predict or describe in detail exotic new properties of nuclei far from the stability valley and to understand the origins of these properties.

For medium-mass and heavy nuclei, an important goal is obtaining a universal energy-density functional, which will be able to describe static and dynamic properties of finite nuclei and extended nucleonic matter with arbitrary neutron-to-proton ratio. Self-consistent methods based on density-functional theory are already sophisticated enough to allow precise analysis of ground-state properties (e.g., binding energies) in heavy nuclei [5–7]. They can also help describe nuclear decays and excited states. Their predictions

for collective excitations as we approach the neutron drip line are especially interesting. But what happens to low- and high-frequency multipole modes when the neutron excess is unusually large?

To address these questions we use the quasiparticle random-phase approximation (QRPA), a powerful tool for understanding both low-lying vibrational states and giant resonances [8]. The QRPA is a microscopic approach that is nevertheless simple enough to allow "no-core" calculations. The approximation, which should be good for collective vibrations as long as their amplitudes are small, is especially effective in conjunction with Skyrme energy functionals. Our work is part of a broad program to test and improve these functionals, which thus far have been fitted mainly to ground-state observables, by applying them to collective excitations, particularly near the drip line. This paper lays out our approach and evaluates its accuracy. For these purposes we restrict ourselves to a single Skyrme functional, SkM*. A forthcoming study will examine the performance of Skyrme functionals more generally.

The QRPA is a standard method for describing collective excitations in open-shell superconducting nuclei with stable mean-field solutions, either spherical or deformed. What is not standard, and at the same time is extremely important for weakly bound nuclei, is the treatment of the particle continuum. Continuum extensions of the random-phase approximation (RPA) or QRPA are usually carried out in coordinate space, facilitating treatment of decay channels and guaranteeing correct asymptotics. Surprisingly, as we discuss

---

*Electronic address: jterasak@physics.unc.edu.
†Electronic address: engelj@physics.unc.edu.
‡Electronic address: mbender@phy.anl.gov.
§Electronic address: dobaczew@fuw.edu.pl.
ᶜElectronic address: witek@utk.edu.
**Electronic address: stoitsovmv@ornl.gov.

in the following, the rich literature on the RPA and QRPA, which includes many coordinate-space calculations, contains few treatments of the continuum that exploit the entire Skyrme functional in a fully self-consistent way.

To avoid confusion, we state what we mean by a fully self-consistent RPA or QRPA calculation. First, the underlying mean-field calculation must be self-consistent in the usual sense. Next, the residual interaction used in the RPA or QRPA must be derived from the same force or energy functional that determines the mean field. An important consequence of this condition, and of other more detailed technical conditions discussed later, is that spurious excitations arising from symmetry breaking by the mean field have zero or nearly zero energy, leaving the physical intrinsic excitations uncontaminated by spurious motion. Finally, energy-weighted sum rules must be satisfied to high accuracy. We elaborate on these requirements in the following; Refs. [9–12] discuss ways in which RPA calculations commonly violate them.

The literature applying RPA or QRPA to nuclear structure is huge, and a complete review is beyond the scope of our paper. We do, however, present an overview of the studies that are related in one way or another to nuclear density functionals, self-consistency, pairing, and the key issue of the particle continuum.

The standard version of QRPA, the so-called matrix formulation, is carried out in the configuration space [13,14] of single-quasiparticle states. A number of papers treat collective states in spherical nuclei in the Skyrme-RPA and QRPA matrix formulation (see Refs. [14,15] and references cited therein), in which the positive-energy continuum is discretized, for example, by solving the Hartree-Fock-Bogoliubov (HFB) and QRPA equations in a harmonic-oscillator single-particle basis. Within this group, the first fully self-consistent calculations that properly account for continuum effects are those of Refs. [16,17], in which the localized canonical basis of coordinate-space HFB is used to calculate β-decay rates of neutron-rich r-process nuclei and Gamow-Teller strength distributions. Recently, fully self-consistent HFB+QRPA calculations have also been carried out with the finite-range Gogny force [18]. Unlike many previous Gogny+HFB studies that employed a harmonic-oscillator basis, Ref. [18] solves the HFB equations in the eigenbasis of a Woods-Saxon potential, the particle continuum of which is discretized by enclosing the system in a box.

Coordinate-space Green's functions as a method of implementing the RPA through linear response were first used in Ref. [19] and subsequently applied to the description of low- and high-energy nuclear modes (see, e.g., Refs. [9,20–29]). Many of those calculations are not realistic enough, however, because they ignore the spin-orbit and Coulomb residual interactions in the RPA [10,11]. Coordinate-space Green's-function QRPA was studied in Ref. [30], in the BCS approximation, with a phenomenological Woods-Saxon average potential. Coordinate-space HFB+QRPA for spherical nuclei was formulated in Refs. [31–34] and applied to excitations of neutron-rich nuclei. As in [30], the Hartree-Fock (HF) field in Refs. [31,32] was approximated by a Woods-Saxon potential. Although the calculations of Refs. [33,34] are based on Skyrme-HFB fields, they violate full self-consistency

by replacing the residual velocity-dependent terms of the Skyrme force by the Landau-Migdal force in the QRPA,[1] and by neglecting spin-spin, spin-orbit, and Coulomb residual interactions entirely. Within this approach, extensive Skyrme-HF+BCS QRPA calculations of $E1$ strength in neutron-rich nuclei were carried out in Refs. [36,37].

An alternative coordinate-representation approach, also based on Green's functions, was formulated in Refs. [38,39] within Migdal's finite-Fermi-systems theory. Most practical applications of this method, however, involve approximations that break self-consistency in one way or another, including the use of highly truncated pairing spaces, different interactions in HFB and QRPA, and the so-called diagonal pairing approximation [38,40–47]. Properties of excited states and strength functions have also been investigated within the relativistic RPA [48–54] or QRPA [55,56]. The QRPA work employs the matrix formulation and is fully self-consistent, since it uses the same Lagrangian in the relativistic Hartree-Bogoliubov calculation of the ground state and in the QRPA matrix equations, which are solved in the canonical basis.

At present, no fully self-consistent continuum HFB+QRPA calculations exist in deformed nuclei. References [57,58] studied giant resonances in deformed nuclei within time-dependent HF theory, formulated in coordinate space with a complex absorbing boundary condition imposed. Symmetry-unrestricted RPA calculations, with no pairing, were carried out in Ref. [59] in a "mixed representation" [60] on a Cartesian mesh in a box, whereas Ref. [61] contains examples of BCS+QRPA calculations in the single-particle basis of a deformed Woods-Saxon potential.

The work described in this paper is essentially fully self-consistent: Among other things we use precisely the same interaction in the HFB and QRPA calculations to preserve the small-amplitude limit of time-dependent HFB. We formulate the QRPA in the canonical eigenbasis of the one-body particle-density matrix [62], which is calculated in the coordinate representation in a large spherical box. As already mentioned, the canonical basis has been used previously to study β decay and Gamow-Teller strength [16,17]; its use in charge-conserving modes near the drip line is more challenging, however, because of the existence of spurious states in the monopole and dipole channels.[2] These zero-energy modes can mix with physical states unless the QRPA equations are solved with high accuracy. We violate full self-consistency very slightly, with negligible consequences for physical states, in our treatment of the 1^- channel (Sec. III B). A less precise implementation of our approach was used to calculate neutrino-nucleus cross sections in ^{208}Pb in Ref. [64].

This paper is organized as follows. Section II presents our approach. In Sec. III we check the QRPA solutions carefully, focusing on spurious modes, and investigate the role of the spin-orbit and Coulomb residual interactions in

---

[1]The treatment of velocity-dependent terms was improved in a recent paper [35].

[2]As far as we know, the only application of the canonical basis to charge-conserving modes near the drip line is in the relativistic QRPA (see, e.g., [55,63]).

the QRPA. Section IV contains the main conclusions of our work. Mathematical details are in two appendixes, the first of which is on the QRPA equations and the second on calculating the derivatives of the Skyrme functionals that enter the formalism.

II. METHOD

Our first step in the self-consistent treatment of excitations is to solve the spherical HFB equations in coordinate space (without mixing neutron and proton quasiparticle wave functions [65]), with the method developed in Ref. [66] (see also Refs. [62,67,68]). We can use arbitrary Skyrme functionals in the particle-hole and pairing (particle-particle) channels.

We modify the code used in Refs. [62,66,67] so that it solves the HFB equations with higher accuracy, which we need because the QRPA uses all the single-quasiparticle states produced by the HFB equations, even those that are essentially unoccupied. Our modifications are to use (i) quadruple precision (though in solving the QRPA equations we use double precision), (ii) a smaller discretization length (0.05 fm), and (iii) a high-quasiparticle-energy cutoff (200 MeV) and a maximum angular momentum $j_{\max} = 15/2$ ($N \leqslant 82$) or $21/2$ ($N > 82$). In a 20-fm box, this cutoff corresponds to 200–300 quasiparticle states for each kind of nucleon. We include all these quasiparticle states in the HFB calculation because a very large energy cutoff is essential for accurate self-consistent QRPA calculations [10]. Hence, the effective pairing window in our HFB calculations is also very large, with the pairing functional fitted to experimental pairing gaps extracted as in Ref. [69] from the measured odd-even mass differences in several Sn, Ni, and Ca isotopes.

Next, we construct the canonical basis, the eigenstates of single-particle density matrix ρ. To avoid poor accuracy (see Ref. [62]) in the wave functions of the nearly empty canonical particle states, we do not diagonalize ρ directly in coordinate space. Instead we construct an intermediate basis by orthonormalizing a set of functions $\{\varphi_1^\mu(\mathbf{r}) + \varphi_2^\mu(\mathbf{r})\}$, where $\varphi_1^\mu(\mathbf{r})$ and $\varphi_2^\mu(\mathbf{r})$ are the upper and lower components of the quasiparticle wave function with energy E_μ [66]. We use the density matrix in coordinate space to calculate the matrix in this basis, which we then diagonalize to obtain the canonical states. The reason for using the sum of $\varphi_1^\mu(\mathbf{r})$ and $\varphi_2^\mu(\mathbf{r})$ is that solutions of the HFB equations expressed in the canonical basis (Eqs. (4.14) of Ref. [62]) are, in the new basis, *guaranteed* to be numerically consistent with those of the original HFB problem. This is because the configuration space is the same in both cases, independent of the pairing cutoff (see Ref. [70] for a discussion relevant to this point). Without pairing, when either $\varphi_1^\mu(\mathbf{r})$ or $\varphi_2^\mu(\mathbf{r})$ is equal to zero, our method is equivalent to taking a certain number of HF states, including many unoccupied states.

In the canonical basis, the HFB+QRPA equations have a form almost identical to that of the BCS+QRPA approximation; the only difference is the presence of off-diagonal terms in the single-quasiparticle energies. The QRPA+HFB formalism employs more pairing matrix elements than the QRPA+BCS, however.

As noted already, full self-consistency requires the use of the same interaction in the QRPA as in the HFB approximation. More specifically, this means that the matrix elements that enter the QRPA equation are related to second derivatives of a mean-field energy functional. We describe the densities and the form of the functional carefully in the appendixes. However, we must meet other conditions as well for QRPA calculation to be self-consistent. Essentially all the single-particle or quasiparticle states produced by the HFB calculation must be used in the space of two-quasiparticle QRPA excitations. This requirement is rather stringent, so we truncate the two-quasiparticle space at several levels and check for convergence of the QRPA solution. First we omit canonical-basis wave functions that have occupation probabilities v_i^2 less than some small v_{crit}^2 (or HF energies greater than some $\varepsilon_{\text{crit}}$ if there is no pairing). Then we exclude from the QRPA pairs of canonical states for which the occupation probabilities are both larger than $1 - v_{\text{crit}}^2$. This second cut is based on the assumption that two-particle transfer modes are not strongly coupled to particle-hole excitations. In addition, if the factors containing u_i and v_i in the QRPA equation—see Eqs. (A12) and (A13)— are very small, in practice smaller than 0.01, then we set the corresponding matrix elements equal to zero. This does not affect the size of the QRPA space, but it significantly speeds up the calculations. For good performance we diagonalize QRPA-Hamiltonian matrices of order 20 000 × 20 000 in neutron-rich Sn isotopes.

Having solved the QRPA equations, we can then calculate the strength function

$$S_J(E) = \frac{1}{\pi} \sum_k \sum_{M=-J}^{J} \frac{\gamma(E_k)|\langle k|\hat{F}_{JM}|0\rangle|^2}{(E_k - E)^2 + \gamma^2(E_k)} \qquad (1)$$

for the multipole operator $\hat{F}_{JM}$. The smoothing width γ is supposed to be large enough to remove spurious oscillations in $S_J(E)$ associated with a finite box radius R_{box} [57,71]. A reasonable form, based on a single-particle estimate, for the smoothing width (Appendix B of Ref. [71]), is

$$\gamma(E) = \begin{cases} \frac{\pi}{R_{\text{box}}}\sqrt{\frac{\hbar^2(E+\lambda_n)}{2m}}, & E \geqslant -\lambda_n, \\ 0.1\,\text{MeV}, & E < -\lambda_n, \end{cases} \qquad (2)$$

where λ_n is the neutron Fermi level and m is the nucleon mass. In deriving Eq. (2) we assumed that the single-proton continuum is effectively shifted up several MeV by the Coulomb barrier. In other words, we associate the threshold energy with the neutron Fermi level. Our prescription is not designed to correct for the absence of spreading and escape widths in the QRPA but rather merely to eliminate artificial peaks associated with the finite box. We do not pretend that measured widths will be the same as those obtained with Eq. (2).

In all the tests in the following, we use the Skyrme functional SkM* [72] and a volume pairing functional [73] [$C^{\tilde{\rho}}(\rho_{00})$, a constant in Eq. (B9)]. The pairing parameter in Eq. (B19) is $V_0 = -77.5$ MeV fm^3. Usually we work in a box of radius 20 fm, though we vary this radius to see its effects. In several tests we examine the weakly bound nucleus
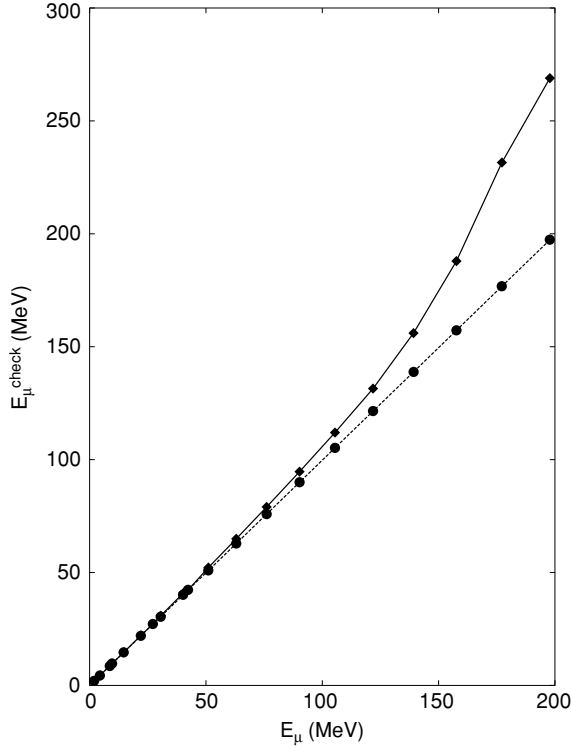
FIG. 1. Neutron quasiparticle energies E_μ^{check} for $s_{1/2}$ states in ^{174}Sn, calculated by diagonalizing the HFB Hamiltonian in the canonical basis, versus the quasiparticle energies E_μ obtained by directly solving the HFB equations in coordinate space. Standard (solid line, diamonds) and improved (dotted line, dots) methods are used to obtain the canonical states. See text for details.

^{174}Sn, which is very close to the two-neutron drip line. In this system, the protons are unpaired and the neutrons paired (with $\Delta_n = 1.016$ MeV) in the HFB ground state.

III. ACCURACY OF SOLUTIONS

Benchmark tests of the HFB part of our calculations are reported in Ref. [74]. Since the accuracy of the canonical wave functions, in which the QRPA calculations are carried out, strongly affects the quality of results (in particular QRPA self-consistency), we take special care to compute them precisely. As discussed in Sec. II, we obtain canonical states by diagonalizing the single-particle density matrix ρ represented in the orthonormalized set of functions $\{\varphi_1^\mu(\mathbf{r}) + \varphi_2^\mu(\mathbf{r})\}$. The accuracy of this method is illustrated in Fig. 1, which plots the quasiparticle energies E_μ^{check}, obtained by diagonalizing the HFB Hamiltonian in the canonical basis [Eq. (4.20) of Ref. [62]], versus the quasiparticle energies E_μ obtained by solving the HFB differential equations directly in coordinate space [Eq. (4.10) of Ref. [62]]. Two sets of canonical states are used: (i) those obtained through the procedure outlined here (dotted line) and (ii) those obtained in the standard way by diagonalizing the density matrix $\rho(\mathbf{r}, \mathbf{r}')$ in discretized coordinate space [Eq. (3.24a) of Ref. [62]; solid line]. If the canonical basis is precisely determined, $E_\mu^{\text{check}} = E_\mu$ and the

TABLE I. The lowest energy excited 0^+ states in ^{174}Sn. The second column shows the excitation energies and the third column the squared matrix elements of the particle-number operator between the kth excited state and the ground state ($k = 0$).

k	E_k (MeV)	$|\langle k|\hat{N}|0\rangle|^2$
1	0.171	0.120
2	2.833	0.533×10^{-5}
3	3.090	0.877×10^{-7}
4	3.810	0.252×10^{-5}
5	3.878	0.480×10^{-5}

two sets of E_μ^{check} coincide. Within the standard approach, however, the high canonical energies deviate visibly from their HFB counterparts; that is, the accuracy of the underlying canonical wave functions is poor. In contrast, the quasiparticle energies and canonical wave functions calculated within the modified approach introduced here are as accurate as the original solutions to the HFB equations, even for high-lying nearly empty states. (See also Sec. VI D of Ref. [75] for a discussion relevant to this point.)

Having examined the canonical basis, we turn to the accuracy of the QRPA part of the calculation. To test it, we first consider solutions related to symmetries. If a Hamiltonian is invariant under a symmetry operator $\hat{P}$ and the HFB state $|\Psi\rangle$ spontaneously breaks the symmetry, then $e^{i\alpha\hat{P}}|\Psi\rangle$, with α an arbitrary c number, is degenerate with the state $|\Psi\rangle$. The QRPA equations have a spurious solution at zero energy associated with the symmetry breaking [8,76], whereas all other solutions are free of the spurious motion. This property is important for strength functions and gives us a way of testing the calculations. Since our QRPA equations, which assume spherical symmetry, are based on mean fields that include pairing and are localized in space, there appears a spurious state associated with particle-number nonconservation (proton and/or neutron; 0^+ channel) and a spurious state associated with center-of-mass motion (1^- channel). These two cases are discussed in Secs. III A and III B.

A. The 0^+ isoscalar mode

In addition to the spurious state associated with nonconservation of particle number by the HFB, the 0^+ channel contains the important "breathing mode." In Table I we display results from a run with $v_{\text{crit}}^2 = 10^{-12}$ for neutrons and $\varepsilon_{\text{crit}} = 150$ MeV for protons, resulting in the inclusion of 310 proton quasiparticle states and the same number of neutron states, with angular momentum up to $j = 21/2$. The table shows the QRPA energies and transition matrix elements of the particle-number operator. The spurious state is below 200 keV, well separated from the other states, all of which have negligible "number strength." The nonzero number strength in the spurious state, like the nonzero energy of that state, is a measure of numerical error. (Both E_k and $|\langle k|\hat{N}|0\rangle|^2$ would be zero for the spurious solution if the calculation were perfect.) If the space of two-quasiparticle states is smaller, with $\varepsilon_{\text{crit}} = 100$ MeV and $v_{\text{crit}}^2 = 10^{-8}$, the energy of the spurious state and the number strength barely change.
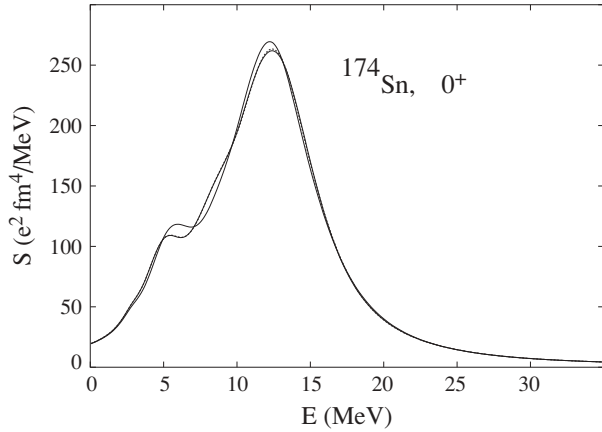
FIG. 2. Isoscalar 0^+ strength function in ^{174}Sn for (i) the single-proton energy cutoff $\varepsilon_{crit} = 100$ MeV and the neutron-quasiparticle occupation cutoff $v^2_{crit} = 10^{-8}$ (thin solid line); (ii) $\varepsilon_{crit} = 150$ MeV and $v^2_{crit} = 10^{-12}$ (dotted line); and (iii) $\varepsilon_{crit} = 200$ MeV and $v^2_{crit} = 10^{-16}$ (thick solid line). Results corresponding to (ii) and (iii) practically coincide.

Figure 2 shows the strength function $S_J(E)$ for the isoscalar 0^+ transition operator (cf. [77])

$$\hat{F}_{00} = \frac{eZ}{A} \sum_{i=1}^{A} r_i^2. \tag{3}$$

We have plotted three curves with successively more quasi-particle levels (from 246 proton levels and 203 neutron levels to 341 proton levels and 374 neutron levels), with cutoff parameters given in the figure caption. The major structures in the strength function are stable. The error remaining after the gentlest truncation is extremely small.

The dependence of the strength function on the box size and quasiparticle cutoff is shown in Fig. 3. The upper part of the figure (panels a–c) corresponds to a constant smoothing width

of $\gamma = 0.5$ MeV. This relatively small value is insufficient to eliminate the finite-box effects but it allows us to assess the stability of the QRPA solutions as a function of R_{box}. The large structure corresponding to the giant monopole resonance (GMR) is independent of box size no matter what the cutoff, but increasing the number of configurations magnifies the dependence on box size of local fluctuations in $S_J(E)$. The curves in the lower part of the figure (panels d–f) are smoothed more realistically, as in Eq. (2). It is gratifying to see that the resulting strength functions are practically identical; that is, the remaining dependence on R_{box} and the cutoff is very weak.

The energy-weighted sum rule (EWSR) for the isoscalar 0^+ mode [77] is given by

$$\sum_k E_k |\langle k|\hat{F}_{00}|0\rangle|^2 = 2\frac{e^2\hbar^2}{m}\frac{Z^2}{A}\langle r^2\rangle, \tag{4}$$

where the expectation value is evaluated in the HFB ground state. This sum rule provides a stringent test of self-consistency in the QRPA. In ^{174}Sn, the right-hand side of Eq. (4) is $35\,215$ e^2 MeV fm^4 and the left-hand side is $34\,985 \pm 15$ e^2 MeV fm^4 for all of the calculations of Fig. 3; the QRPA strength essentially exhausts the sum rule. (The QRPA values of the EWSR in this paper are obtained by summing up to $E_k = 50$ MeV.)

B. The isoscalar 1^- mode

The 1^- channel, home of the giant dipole resonance, the isoscalar squeezing resonance, and as yet incompletely understood low-energy peaks in neutron-rich nuclei (sometimes associated with skin excitations), has a spurious isoscalar mode associated with center-of-mass motion that can seriously compromise the low-energy spectrum if not handled with extreme care. In our implementation of QRPA, the spurious mode has an energy that is not quite zero because we violate
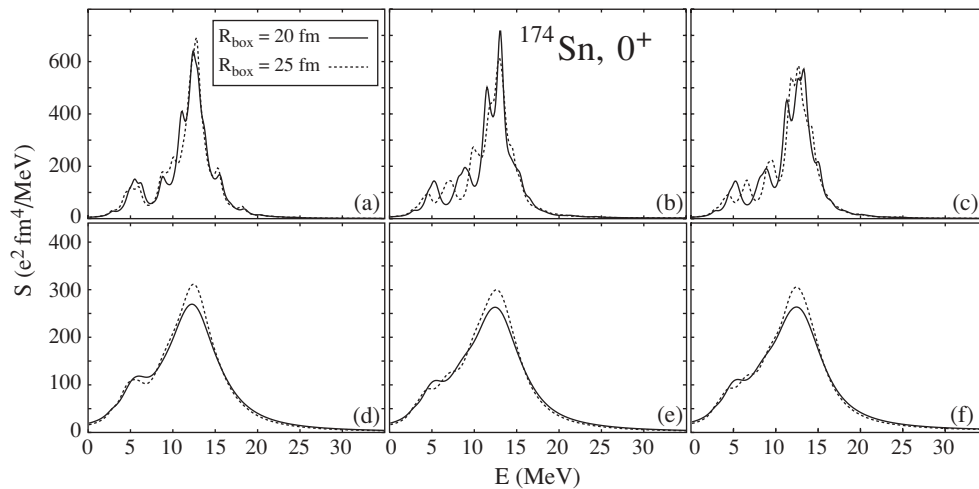

FIG. 3. Isoscalar 0^+ strength function in ^{174}Sn for the box radii: $R_{box} = 20$ fm (solid line) and $R_{box} = 25$ fm (dotted line). In (a), (b), and (c) the smoothing-width parameter γ is 0.5 MeV for all energies, whereas in (d), (e), and (f) $\gamma(E)$ is given by Eq. (2). We use the same three sets of cutoff conditions as in Fig. 2, namely (i) in parts (a) and (d), (ii) in parts (b) and (e), and (iii) in parts (c) and (f).
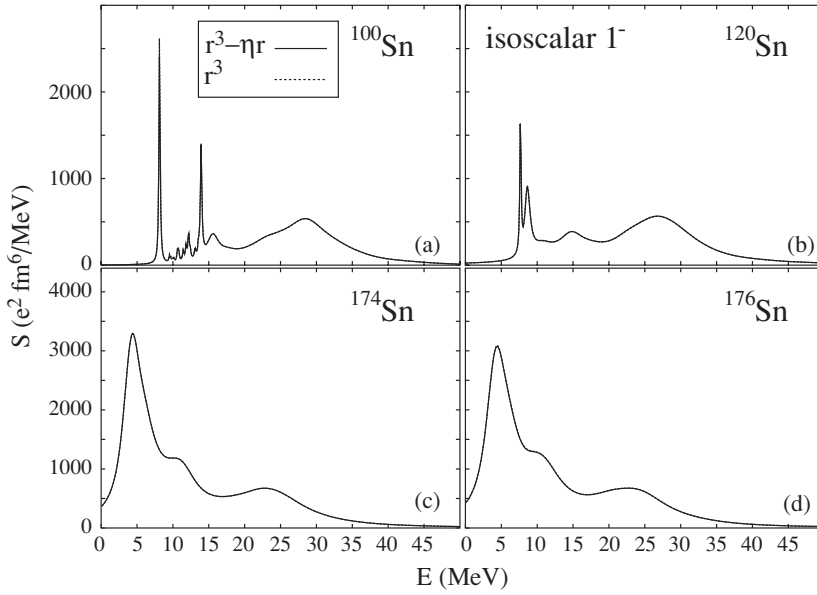
FIG. 4. Isoscalar 1^- strength function in ^{100,120,174,176}Sn for the corrected dipole operator in Eq. (6) (solid line) and the uncorrected operator in Eq. (5) (dotted line). The cutoff $\varepsilon_{\text{crit}}$ is 140 MeV, and v_{crit}^2 is 3×10^{-12}. The self-consistency of our calculations makes the solid and dotted curves coincide nearly exactly over the whole energy range.

translational invariance slightly in two ways: First, by adopting the box boundary condition we assume the presence of an external one-body potential that encloses the system. This infinite square well is manifestly not translationally invariant (see, e.g., relevant discussion in Sec. 3.5 of Ref. [12]). Second, the energy cutoff imposed on the single-quasiparticle spectrum at the HFB level prevents us—by breaking the closure relation for canonical states—from exactly expressing what would be the spurious state in a translationally invariant calculation (i.e., the momentum operator acting on the HFB ground state) in terms of our QRPA excitations [12]. As we now show, however, the effects of the explicit violation are small, particularly in the physical-state energies and wave functions.

We examine the properties of the resulting spurious mode in ^{100}Sn, ^{120}Sn, ^{174}Sn, and ^{176}Sn. (The nuclei ^{100}Sn and ^{176}Sn are the two-proton and two-neutron drip-line systems predicted by the HFB calculation with SkM*. Neither nucleus has any static pairing; i.e., $\Delta_n = \Delta_p = 0$.) In the following calculations, we take $\varepsilon_{\text{crit}} = 140$ MeV for the protons and $v_{\text{crit}}^2 = 9 \times 10^{-12}$ for the neutrons. As already discussed, smoothed strength functions are practically independent of small changes in the cutoff. They are also independent of the cutoff in quasiparticle angular momentum provided we include all states with $j \leqslant 15/2$.

Figure 4 shows the predicted isoscalar dipole strength function for ^{100,120,174,176}Sn. For the transition operator, we use

$$\hat{F}_{1M} = \frac{eZ}{A} \sum_{i=1}^{A} r_i^3 Y_{1M}(\Omega_i), \tag{5}$$

and we use the corrected operator

$$\hat{F}_{1M}^{\text{cor}} = \frac{eZ}{A} \sum_{i=1}^{A} \left(r_i^3 - \eta r_i \right) Y_{1M}(\Omega_i), \quad \eta = \frac{5}{3} \langle r^2 \rangle, \tag{6}$$

to remove as completely as possible residual pieces of the spurious state from the physical states [10]. The fact that the strength functions produced by these two operators—displayed in Fig. 4—coincide so closely shows both the unimportance of the explicit violation of translational invariance and the extreme accuracy of our QRPA solutions; they are essentially uncontaminated by spurious motion even without the operator correction. The spurious-state energies E_{spurious} are 0.964 MeV for ^{100}Sn and 0.713 MeV for ^{120}Sn, and the energies of the first physical excited states are 7.958 MeV for ^{100}Sn and 7.729 MeV for ^{120}Sn. In ^{174}Sn (^{176}Sn), E_{spurious} is 0.319 MeV (0.349 MeV) and the first physical state is at 3.485 MeV (2.710 MeV), lower than in the more stable isotopes. Pairing correlations do not affect accuracy; the neutrons in ^{120}Sn and ^{174}Sn are paired, whereas those in ^{100}Sn and ^{176}Sn are not.

As a final check on the separation of center-of-mass motion, we calculated the transition density

$$\rho_{\text{tr}}(r; k) = r^2 \int d\Omega \, Y_{1M}(\Omega) \langle k | \sum_{i=1}^{A} \delta(\boldsymbol{r} - \boldsymbol{r}_i) | 0 \rangle \tag{7}$$

for the spurious state, which ideally should be proportional to $r^2 \frac{d\rho(r)}{dr}$ [10], where $\rho(r)$ is the ground-state density in the HFB approximation. The top half of Fig. 5 shows our QRPA result, which is indistinguishable from the HFB derivative. To see the size of deviations, we plotted the difference between the two curves (with the constant of proportionality fixed at $r = 6.5$ fm, an arbitrary point) with a magnified scale in the bottom half of the figure. The spurious-state transition density is very accurate.

We display the fine structure of the isoscalar 1^- strength functions in ^{120}Sn and ^{174}Sn in Fig. 6, which also illustrates the dependence of the results on R_{box}. The dependence is consistent with that of Fig. 3 for the isoscalar 0^+ strength; the low-amplitude fluctuations in $S_J(E)$ that are unstable as a function of R_{box} disappear, and the smoothed strength function
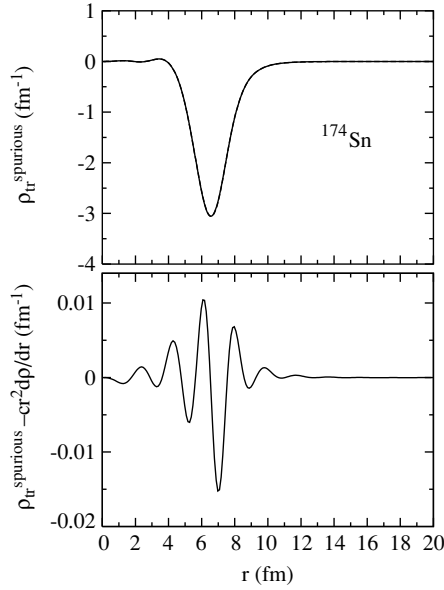
FIG. 5. Transition density of the spurious 1^- state and the indistinguishable curve $cr^2 \, d\rho(r)/dr$ (upper panel), and the difference between the two curves (lower panel). The line thickness in the upper panel is about 0.01 fm^{-1}. The constant c is fixed at $r = 6.5$ fm.

depends only weakly on R_{box}. In ^{120}Sn, the two sharp peaks below 10 MeV correspond to discrete states, whereas the broad maxima centered around 15 and 27 MeV are in the continuum, well above the neutron-emission threshold. A similar three-peaked structure emerges in ^{174}Sn, though most of the strength there is concentrated in the low-energy peak at $E \approx 4$ MeV. Figure 4 shows (as we will discuss in our forthcoming paper [78]) that the appearance of the low-energy isoscalar dipole strength is a real and dramatic feature of neutron-rich drip-line nuclei [79,80].
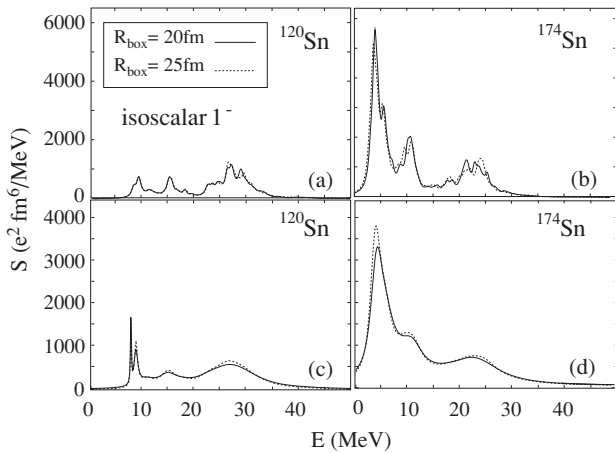
FIG. 6. Isoscalar 1^- strength function in ^{120}Sn (left) and ^{174}Sn (right) for two box radii: $R_{\text{box}} = 20$ fm (solid line) and $R_{\text{box}} = 25$ fm (dotted line). In (a) and (b) the smoothing-width parameter is constant ($\gamma = 0.5$ MeV), whereas in (c) and (d) $\gamma(E)$ is given by Eq. (2).

The EWSR for the isoscalar 1^- mode [77] is

$$\sum_k \sum_M E_k \left| \langle k | \hat{F}_{1M}^{\text{cor}} | 0 \rangle \right|^2 = \frac{3}{8\pi} \frac{e^2 \hbar^2}{m} \frac{Z^2}{A} \left(11 \langle r^4 \rangle - \frac{25}{3} \langle r^2 \rangle^2 \right). \tag{8}$$

In ^{174}Sn, the right-hand side is $403\,310\ e^2$ MeV fm^6, whereas the left-hand side is $400\,200\ e^2$ MeV fm^6. For ^{176}Sn, the corresponding numbers are $406\,576\ e^2$ MeV fm^6 and $407\,100\ e^2$ MeV fm^6. This level of agreement is very good.

C. The isovector 0^+ and isoscalar, isovector 2^+ modes

Figure 7 displays strength functions for the 0^+ and 2^+ channels in ^{120}Sn and ^{174}Sn. (We discussed the isoscalar 0^+ mode first to illustrate the accuracy of our solutions, but we include it here as well for completeness.) The calculations show the appearance of low-energy 0^+ strength—both isovector and isoscalar—and low-energy isovector 2^+ strength in ^{174}Sn, though in none of these instances is the phenomenon quite as dramatic as in the isoscalar 1^- channel.

The EWSR for the isoscalar 2^+ transition operator,

$$\hat{F}_{2M} = e \frac{Z}{A} \sum_{i=1}^{A} r_i^2 Y_{2M}(\Omega_i), \tag{9}$$

can be written as [77]

$$\sum_k \sum_M E_k |\langle k | \hat{F}_{2M} | 0 \rangle|^2 = \frac{25}{4\pi} \frac{e^2 \hbar^2}{m} \frac{Z^2}{A} \langle r^2 \rangle. \tag{10}$$

The sum rule is obeyed as well in the 2^+ isoscalar channel as in the 0^+ and 1^- channels; the only difference is that one needs to include quasiparticle states with $j > 15/2$ for ^{174}Sn. For ^{120}Sn (^{174}Sn) from Fig. 7, the EWSR is $37\,222\ (34\,971)$ e^2 MeV fm^4, whereas the QRPA value is $37\,030\ (35\,010)$ e^2 MeV fm^4.

While on the topic of the sum rule, we display in Table II the j_{max} dependence of the EWSR for several channels in ^{150}Sn, with $R_{\text{box}} = 25$ fm. By taking $j_{\text{max}} = 19/2$ we appear to obtain essentially the entire strength in all three cases. Finally, we note that the lowest 2^+ state of ^{120}Sn has $E = 1.205$ MeV and $B(E2; 0^+ \rightarrow 2^+) = 3077\ e^2$ fm^4 in our calculation, whereas the experimental data are $E = 1.171$ MeV and $B(E2; 0^+ \rightarrow 2^+) = 2020 \pm 40\ e^2$ fm^4 [81]. We will make more extensive comparisons in a future paper.

TABLE II. The j_{max} dependence of isoscalar EWSR for ^{150}Sn. R_{box} is 25 fm.

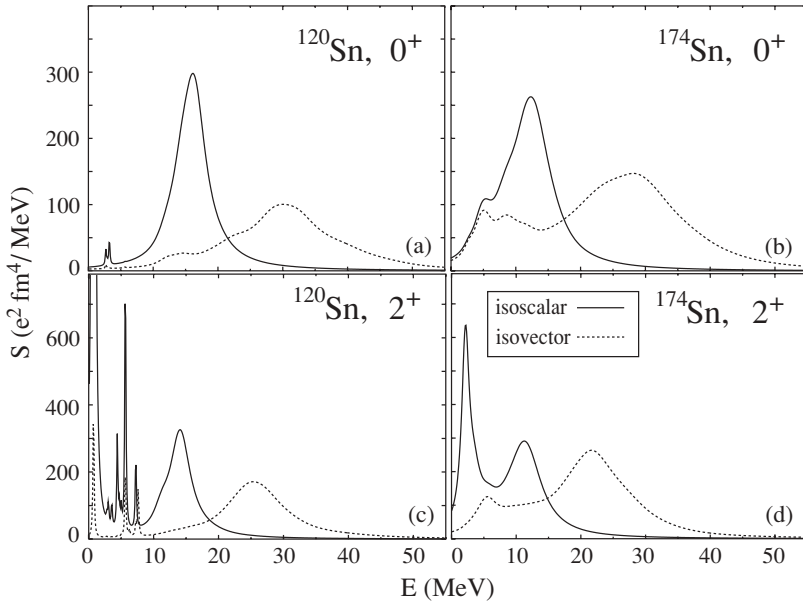| $T J^\pi$	Units	$j_{\text{max}} = 19/2$	$j_{\text{max}} = 25/2$
IS 0^+	e^2 MeV fm^4	35 731	35 633
IS 1^-	e^2 MeV fm^6	361 686	353 936
IS 2^+	e^2 MeV fm^4	35 542	35 445

FIG. 7. Isoscalar and isovector strength functions for (a) the 0^+ channel of ^{120}Sn, (b) the 0^+ channel of ^{174}Sn, (c) the 2^+ channel of ^{120}Sn, and (d) the 2^+ channel of ^{174}Sn. The cutoff $\varepsilon_{\rm crit}$ is 150 MeV and $v_{\rm crit}^2$ is 10^{-12}.

D. Calculations without the spin-orbit or Coulomb residual interactions

Since many existing QRPA calculations omit the spin-orbit and Coulomb interactions, as discussed in the Introduction, we examine the strength functions with and without these terms to see how large an error their omission causes. We performed QRPA calculations in the $J^\pi = 0^+, 1^-$, and 2^+ channels in ^{120,174}Sn, omitting the two interactions in turn while keeping all terms in the HFB. Figure 8 shows the results in the 0^+ channel. When we omit the spin-orbit residual interaction the peak energy is shifted up about 300 keV and the peak height is lowered by 15%; the effect of omitting the Coulomb residual interaction is smaller. The change in the EWSR is less than 1% in either case. The discrepancies in the strength functions

of the other modes are similar, though sometimes less. In any event, the errors induced by omitting such terms are much larger than the small ones we make by truncating our canonical basis.

How is the spurious strength affected by the removal of, for example, the spin-orbit term in the residual interaction? We found that although 0^+ spurious strength remains highly concentrated in one state, the 1^- spurious strength spreads appreciably near the neutron drip line, as shown by Fig. 9, which was obtained by omitting the spin-orbit interaction. The corrected strength function is similar to that of Fig. 4(c), but the uncorrected function, which was identical to its corrected counterpart in Fig. 4(c), is now quite different.
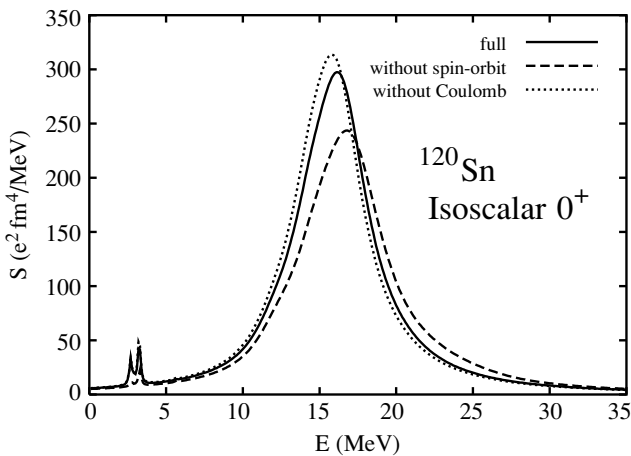

FIG. 8. Isoscalar 0^+ strength functions in ^{120}Sn without the residual spin-orbit interaction in the QRPA (dashed curve), without the residual Coulomb interaction (dotted curve), and with all terms included (solid curve).
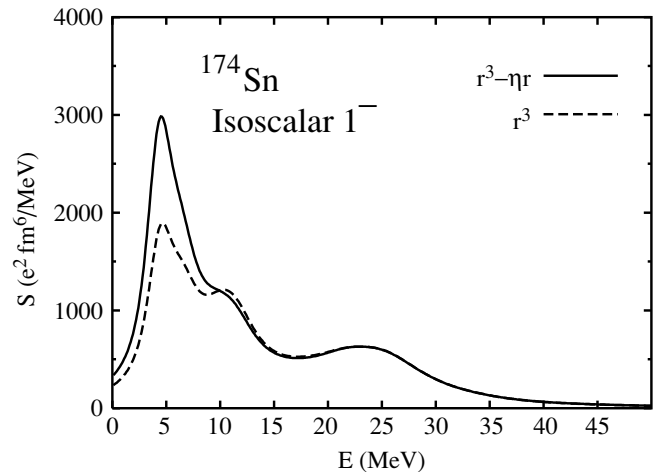

FIG. 9. Isoscalar 1^- strength functions in ^{174}Sn without the spin-orbit residual interaction, with and without the correction to remove spurious strength.

IV. CONCLUSION

In this work we have reported on the development and detailed testing of a fully self-consistent Skyrme-QRPA framework that employs the canonical HFB basis. The method can be used to calculate strength distributions in any spin-isospin channel and in any spherical even-even nucleus. A good calculation requires a large single-quasiparticle space. Our results show that our space is large enough in nuclei as heavy as the Sn isotopes.

We are currently investigating the predictions of a range of Skyrme functionals across the Ca, Ni, and Sn isotope chains. The initial results presented here point to increases in low-lying strength at the neutron drip line, particularly in the isoscalar-dipole channel. In a forthcoming paper [78] we will report on the robustness of these effects, on the physics underlying them, on their variation with atomic mass and number, and on their implications for the future of Skyrme functionals.

APPENDIX A: QRPA EQUATION

The QRPA equations are the small-oscillations limit of the time-dependent Hartree-Fock-Bogoliubov approximation (see, e.g., [8,14]). In the canonical basis the most general equations take the form

$$\sum_{L < L'} \begin{pmatrix} A_{KK',LL'} & B_{KK',LL'} \\ -B^*_{KK',LL'} & -A^*_{KK',LL'} \end{pmatrix} \begin{pmatrix} X^k_{LL'} \\ Y^k_{LL'} \end{pmatrix} = E_k \begin{pmatrix} X^k_{KK'} \\ Y^k_{KK'} \end{pmatrix},$$
$$K < K', \tag{A1}$$

$$A_{KK',LL'} = E_{KL}\delta_{K'L'} - E_{K'L}\delta_{KL'} - E_{KL'}\delta_{K'L} + E_{K'L'}\delta_{KL}$$
$$- \bar{V}^{\text{ph}}_{K\bar{L}\bar{K}'L'} u_L v_L u_K v_{K'} + \bar{V}^{\text{ph}}_{K'\bar{L}\bar{K}L'} u_L v_L u_{K'} v_K$$

$$+ \bar{V}^{\text{ph}}_{K\bar{L}'\bar{K}'L} u_L v_{L'} u_K v_{K'} - \bar{V}^{\text{ph}}_{K'\bar{L}'\bar{K}L} u_L v_{L'} u_{K'} v_K$$
$$- \bar{V}^{\text{pp}}_{\bar{L}\bar{L}'\bar{K}'\bar{K}} v_L v_{L'} v_K v_{K'} - \bar{V}^{\text{pp}}_{KK'L'L} u_K u_{K'} u_L u_{L'}$$
$$- \bar{V}^{\text{3p1h}}_{\bar{L}\bar{L}'K\bar{K}'} v_L v_{L'} u_K v_{K'} + \bar{V}^{\text{3p1h}}_{\bar{L}\bar{L}'K'\bar{K}} v_L v_{L'} u_{K'} v_K$$
$$- \bar{V}^{\text{3p1h}}_{KK'\bar{L}L} u_K u_{K'} u_L v_L + \bar{V}^{\text{3p1h}}_{KK'\bar{L}'L} u_K u_{K'} u_L v_{L'}$$
$$- \bar{V}^{\text{1p3h}}_{\bar{L}L'\bar{K}'\bar{K}} u_L v_L v_{K'} v_K + \bar{V}^{\text{1p3h}}_{\bar{L}'L\bar{K}'\bar{K}} u_L v_{L'} v_{K'} v_K$$
$$- \bar{V}^{\text{1p3h}}_{K\bar{K}'L'L} u_K v_{K'} u_L u_{L'} + \bar{V}^{\text{1p3h}}_{K'\bar{K}L'L} u_{K'} v_K u_L u_{L'}, \tag{A2}$$

$$B_{KK',LL'} = \bar{V}^{\text{ph}}_{K'L'\bar{K}\bar{L}} u_L v_L u_{K'} v_K - \bar{V}^{\text{ph}}_{KL'\bar{K}'\bar{L}} u_L v_L u_K v_{K'}$$
$$- \bar{V}^{\text{ph}}_{K'L\bar{K}\bar{L}'} u_L v_{L'} u_{K'} v_K + \bar{V}^{\text{ph}}_{KL\bar{K}'\bar{L}'} u_L v_{L'} u_K v_{K'}$$
$$+ \bar{V}^{\text{pp}}_{K'K\bar{L}\bar{L}'} v_L v_{L'} u_K u_{K'} + \bar{V}^{\text{pp}}_{L'L\bar{K}\bar{K}'} v_K v_{K'} u_L u_{L'}$$
$$+ \bar{V}^{\text{3p1h}}_{K'KL'\bar{L}} u_L v_L u_K u_{K'} - \bar{V}^{\text{3p1h}}_{K'KL\bar{L}'} u_L v_{L'} u_K u_{K'}$$
$$+ \bar{V}^{\text{3p1h}}_{L'LK'\bar{K}} u_{K'} v_K u_L u_{L'} - \bar{V}^{\text{3p1h}}_{L'LK\bar{K}'} u_K v_{K'} u_L u_{L'}$$
$$+ \bar{V}^{\text{1p3h}}_{K'\bar{K}\bar{L}\bar{L}'} v_L v_{L'} u_{K'} v_K - \bar{V}^{\text{1p3h}}_{K\bar{K}'\bar{L}\bar{L}'} v_L v_{L'} u_K v_{K'}$$
$$+ \bar{V}^{\text{1p3h}}_{L'\bar{L}\bar{K}\bar{K}'} v_K v_{K'} u_L v_L - \bar{V}^{\text{1p3h}}_{L\bar{L}'\bar{K}\bar{K}'} v_K v_{K'} u_L v_{L'}, \tag{A3}$$

$$\bar{V}^{\text{ph}}_{KLK'L'} = \frac{\delta^2 E[\rho, \kappa, \kappa^*]}{\delta\rho_{K'K}\delta\rho_{L'L}}, \tag{A4}$$

$$\bar{V}^{\text{pp}}_{K'KL'L} = \frac{\delta^2 E[\rho, \kappa, \kappa^*]}{\delta\kappa^*_{K'K}\delta\kappa_{L'L}}, \tag{A5}$$

$$\bar{V}^{\text{3p1h}}_{K'KL'L} = \frac{\delta^2 E[\rho, \kappa, \kappa^*]}{\delta\kappa^*_{K'K}\delta\rho_{LL'}} = \bar{V}^{\text{1p3h}*}_{LL'K'K}, \tag{A6}$$

where K and L are single-particle indices for the canonical basis, and the states are assumed to be ordered. The symbol $\bar{K}$ refers to the conjugate partner of K, u_K and v_K come from the BCS transformation associated with the canonical basis, and the E_{KL} are the one-quasiparticle matrix elements of the HFB Hamiltonian [cf. Eq. (4.14b) of Ref. [62]]. $X^k_{LL'}$ and $Y^k_{LL'}$ are the forward and backward amplitudes of the QRPA solution k, and E_k is the corresponding excitation energy. $E[\rho, \kappa, \kappa^*]$ is the energy functional (see Appendix B for an explicit definition) and ρ and κ are the density matrix and pairing tensor, respectively. After taking the functional derivatives, we replace ρ and κ by their HFB solutions, in complete analogy with an ordinary Taylor-series expansion.

To write the equations in coupled form, we introduce the notation

$$K \equiv (n_\mu l_\mu j_\mu m_\mu) \equiv (\mu m_\mu), \quad L \equiv (\nu m_\nu), \tag{A7}$$

where $(nljm)$ denote spherical quantum numbers. Using (i) rotational, time-reversal, and parity symmetries of the HFB state, (ii) the conjugate single-particle state[3]

$$|\overline{K}\rangle = |\overline{\mu m_\mu}\rangle = (-)^{j_\mu - m_\mu} |\mu - m_\mu\rangle, \tag{A8}$$

---

[3]The conjugate state in our HFB code is slightly different: $|\overline{\mu m}\rangle = (-)^{j-m+l}|\mu - m\rangle$. This definition follows from Eq. (3.24b) of Ref. [62] and the single-particle wave function $\psi_{\mu m}(\mathbf{r}) = R_\mu(r)\sum_{l_z\sigma} Y_{ll_z}(\Omega)\langle ll_z\frac{1}{2}\sigma|jm\rangle|\sigma\rangle$, where $R_\mu(r)$ and $|\sigma = \pm 1/2\rangle$ are real radial and spin wave functions, respectively. Thus, we multiply all HFB v_μ by $(-)^l$ in the QRPA calculations.

and (iii) the relations

$$X^k_{KK'} = \langle j_\mu m_\mu j_{\mu'} m_{\mu'} | J_k M_k \rangle \bar{X}^k_{[\mu\mu']J_k} \times \begin{cases} \sqrt{2}, & \mu = \mu', \\ 1, & \text{otherwise}, \end{cases}$$
(A9)

$$Y^k_{KK'} = (-)^{j_\mu - m_\mu}(-)^{j_{\mu'} - m_{\mu'}} \langle j_\mu - m_\mu j_{\mu'} - m_{\mu'} | J_k M_k \rangle$$
$$\times \bar{Y}^k_{[\mu\mu']J_k} \times \begin{cases} \sqrt{2}, & \mu = \mu', \\ 1, & \text{otherwise}, \end{cases}$$
(A10)

with J_k the angular momentum of the state k and the factor $\sqrt{2}$ for convenience [13], one can rewrite the QRPA equation as

$$\sum_{\nu \leqslant \nu'} \begin{pmatrix} A_{[\mu\mu']J_k,[\nu\nu']J_k} & B_{[\mu\mu']J_k,[\bar{\nu}\bar{\nu}']J_k} \\ -B^*_{[\mu\mu']J_k,[\bar{\nu}\bar{\nu}']J_k} & -A^*_{[\mu\mu']J_k,[\nu\nu']J_k} \end{pmatrix} \begin{pmatrix} \bar{X}^k_{[\nu\nu']J_k} \\ \bar{Y}^k_{[\nu\nu']J_k} \end{pmatrix}$$

$$= E_k \begin{pmatrix} \bar{X}^k_{[\mu\mu']J_k} \\ \bar{Y}^k_{[\mu\mu']J_k} \end{pmatrix}, \quad \mu \leqslant \mu',$$
(A11)

$$A_{[\mu\mu']J_k,[\nu\nu']J_k} = \frac{1}{\sqrt{1+\delta_{\mu\mu'}}} \frac{1}{\sqrt{1+\delta_{\nu\nu'}}}$$
$$\times \{ E_{\mu\nu}\delta_{\mu'\nu'} - E_{\mu'\nu}\delta_{\mu\nu'}(-)^{j_\mu + j_{\mu'} - J_k}$$
$$- E_{\mu\nu'}\delta_{\mu'\nu}(-)^{j_\mu + j_{\mu'} - J_k} + E_{\mu'\nu'}\delta_{\mu\nu}$$
$$+ G(\mu\mu'\nu\nu'; J_k)(u_{\mu'}u_\mu u_\nu u_{\nu'} + v_\nu v_{\nu'} v_\mu v_\mu)$$
$$+ F(\mu\mu'\nu\nu'; J_k)(u_\mu v_{\nu'}u_\nu v_{\mu'} + u_{\mu'}v_\nu u_{\nu'}v_\mu)$$
$$- (-)^{j_{\nu'}+j_\nu - J_k}F(\mu\mu'\nu'\nu; J_k)(u_\mu v_\nu u_{\nu'} v_{\mu'}$$
$$+ u_{\mu'}v_{\nu'}u_\nu v_\mu) - H(\mu\mu'\nu\nu'; J_k)(v_\nu v_{\nu'}u_\mu v_{\mu'}$$
$$+ u_{\mu'}v_\mu u_\nu u_{\nu'}) + (-)^{j_\mu + j_{\mu'} - J_k}H(\mu'\mu\nu\nu'; J_k)$$
$$\times (v_\nu v_{\nu'}u_{\mu'}v_\mu + u_\mu v_{\mu'}u_\nu u_{\nu'})$$
$$- H^*(\nu\nu'\mu\mu'; J_k)(u_\mu u_{\mu'}u_\nu v_\nu + u_\nu v_{\nu'}v_{\mu'}v_\mu)$$
$$+ (-)^{j_\nu + j_{\nu'} - J_k}H^*(\nu'\nu\mu\mu'; J_k)(u_\mu u_{\mu'}u_\nu v_{\nu'}$$
$$+ u_{\nu'}v_\nu v_{\mu'}v_\mu) \},$$
(A12)

$$B_{[\mu\mu']J_k,[\bar{\nu}\bar{\nu}']J_k} = \frac{1}{\sqrt{1+\delta_{\mu\mu'}}} \frac{1}{\sqrt{1+\delta_{\nu\nu'}}}$$
$$\times \{ -G(\mu\mu'\nu\nu'; J_k)(u_{\mu'}u_\mu v_\nu v_{\nu'}$$
$$+ u_\nu u_{\nu'}v_{\mu'}v_\mu) - (-)^{j_\nu + j_{\nu'} - J_k}$$
$$\times F(\mu\mu'\nu'\nu; J_k)(u_\mu u_\nu v_{\mu'}v_{\nu'} + u_{\mu'}u_{\nu'}v_\nu v_\mu)$$
$$+ (-)^{j_\nu + j_{\nu'} + j_\mu + j_{\mu'}}F(\mu'\mu\nu'\nu; J_k)(u_\mu u_\nu v_{\nu'}v_\mu$$
$$+ u_\mu u_{\nu'}v_{\mu'}v_\nu) + H(\mu\mu'\nu\nu'; J_k)$$
$$\times (v_\nu v_{\nu'}u_{\mu'}v_\mu + u_\mu v_{\mu'}u_\nu u_{\nu'})$$
$$- (-)^{j_\mu + j_{\mu'} - J_k}H(\mu'\mu\nu\nu'; J_k)(v_\nu v_{\nu'}u_\mu v_{\mu'}$$
$$+ u_{\mu'}v_\mu u_\nu u_{\nu'}) - H^*(\nu\nu'\mu\mu'; J_k)$$
$$\times (v_\mu v_{\mu'}u_\nu v_\nu + u_\nu v_{\nu'}u_\mu u_{\mu'}) + (-)^{j_\nu + j_{\nu'} - J_k}$$
$$\times H^*(\nu'\nu\mu\mu'; J_k)(v_\mu v_{\mu'}u_\nu v_{\nu'} + u_{\nu'}v_\nu u_\mu u_{\mu'}) \},$$
(A13)

$$G(\mu\mu'\nu\nu'; J_k) = \sum_{m_\mu m_{\mu'} m_\nu m_{\nu'}} \langle j_\mu m_\mu j_{\mu'} m_{\mu'} | J_k M_k \rangle$$
$$\times \langle j_\nu m_\nu j_{\nu'} m_{\nu'} | J_k M_k \rangle \bar{V}^{\text{pp}}_{KK'LL'}$$
$$\equiv \langle [\mu\mu']J_k | \bar{V}^{\text{pp}} | [\nu\nu']J_k \rangle,$$
(A14)

$$F(\mu\mu'\nu\nu'; J_k) = \sum_{m_\mu m_{\mu'} m_\nu m_{\nu'}} \langle j_\mu m_\mu j_{\mu'} m_{\mu'} | J_k M_k \rangle$$
$$\times \langle j_\nu m_\nu j_{\nu'} m_{\nu'} | J_k M_k \rangle \bar{V}^{\text{ph}}_{K\bar{L}'\bar{K}'L}$$
$$= \sum_{J'} (-)^{j_{\mu'}+j_\nu + J'} \begin{Bmatrix} j_\mu & j_{\mu'} & J_k \\ j_\nu & j_{\nu'} & J' \end{Bmatrix} (2J'+1)$$
$$\times \langle [\mu\nu']J_k | \bar{V}^{\text{ph}} | [\mu'\nu]J_k \rangle,$$
(A15)

$$H(\mu\mu'\nu\nu'; J_k) = \sum_{m_\mu m_{\mu'} m_\nu m_{\nu'}} \langle j_\mu m_\mu j_{\mu'} m_{\mu'} | J M \rangle$$
$$\times \langle j_\nu m_\nu j_{\nu'} m_{\nu'} | J M \rangle \bar{V}^{\text{3p1h}}_{\bar{L}\bar{L}'K\bar{K}'}$$
$$= \sum_{J'} (-)^{j_\mu + j_\nu + 1 + l_{\nu'} - J_k - J'} \begin{Bmatrix} j_\mu & j_{\mu'} & J_k \\ j_{\nu'} & j_\nu & J' \end{Bmatrix}$$
$$\times (2J'+1)\langle [\mu\nu]J_k | \bar{V}^{\text{3p1h}} | [\mu'\nu']J_k \rangle.$$
(A16)

We have represented the second derivatives of the energy functional $E[\rho, \kappa, \kappa^*]$ as matrix elements of effective interactions $\bar{V}^{\text{pp}}$, $\bar{V}^{\text{ph}}$, and $\bar{V}^{\text{3p1h}}$; only the matrix elements of the first are antisymmetrized if the interaction is density dependent. The effective interactions themselves are given in Appendix B. Although some of the "matrix elements" are unsymmetrized, the underlying two-quasiparticle states are of course antisymmetric. As a consequence, $A_{[\mu\mu']J_k,[\nu\nu']J_k} = B_{[\mu\mu']J_k,[\bar{\nu}\bar{\nu}']J_k} = 0$ if J_k is odd and either $\mu = \mu'$ or $\nu = \nu'$.

The nuclear energy functional $E[\rho, \kappa, \kappa^*]$ is usually separated into particle-hole (ph) and pairing pieces (again, see Appendix B for explicit expressions). If the pairing functional, which we will call $E_{\text{pair}}[\rho, \kappa, \kappa^*]$, depends on ρ then the derivatives of $E_{\text{pair}}[\rho, \kappa, \kappa^*]$ with respect to $\rho_{KK'}$ are called pairing-rearrangement terms [14]. In the QRPA, two kinds of pairing-rearrangement terms can arise in general. One has particle-hole character and is included in $\bar{V}^{\text{ph}}_{KLK'L'}$; the other affects 3-particle-1-hole (3p1h) and 1-particle-3-hole (1p3h) configurations and is represented by $\bar{V}^{\text{3p1h}}_{K'KL'L}$ and $\bar{V}^{\text{1p3h}}_{K'KL'L}$. If the ρ dependence of $E_{\text{pair}}[\rho, \kappa, \kappa^*]$ is linear, then the ph-type pairing-rearrangement term does not appear. Furthermore, the 3p1h and 1p3h pairing-rearrangement terms arise only for $J^\pi = 0^+$ modes if the HFB state has $J = 0$. Most existing work uses a pairing functional that is linear in ρ, and so needs no pairing-rearrangement terms in $J^\pi \neq 0^+$ channels.

APPENDIX B: INTERACTION MATRIX ELEMENTS (SECOND FUNCTIONAL DERIVATIVES)

1. Representation of second derivatives as matrix element of effective interactions

In this Appendix, we discuss interaction matrix elements coming from $E[\rho, \kappa, \kappa^*]$, which we take to contain separate Skyrme (i.e., strong-force, κ-independent), Coulomb, and pairing energy functionals:

$$E[\rho, \kappa, \kappa^*] = E_{\text{Skyrme}}[\rho] + E_{\text{Coul}}[\rho_p] + E_{\text{pair}}[\rho, \kappa, \kappa^*],$$
(B1)

where ρ_p is the proton density matrix. The most general Skyrme energy functional in common use is given by

$$E_{\text{Skyrme}}[\rho] = \sum_{t=0,1} \int d^3r \big\{ C_t^\rho[\rho_{00}]\, \rho_{t0}^2(r) + C_t^{\Delta\rho} \rho_{t0}(r)\Delta\rho_{t0}(r)$$

$$+ C_t^\tau \big[\rho_{t0}(r)\,\tau_{t0}(r) - j_{t0}^2(r)\big]$$

$$+ C_t^s[\rho_{00}]\, s_{t0}^2(r) + C_t^{\Delta s} s_{t0}(r)\cdot\Delta s_{t0}(r)$$

$$+ C_t^T \big[s_{00}(r)\cdot T_{t0}(r) - \overset{\leftrightarrow}{J}{}_{t0}^2(r) \big] + C_t^{\nabla J}$$

$$\times [\rho_{t0}(r)\nabla\cdot J_{t0}(r) + s_{t0}(r)\cdot\nabla\times j_{t0}(r)]\big\}. \tag{B2}$$

(See, e.g., [65,82,83] and references therein for a general discussion.) All densities are labeled by isospin indices tt_z, where t takes values zero and one and t_z is always equal to zero. A more general theory could violate isospin at the single-quasiparticle level, leading to additional densities $\rho_{1\pm1}$ [65]. We do not consider such densities here. The C_t^i are the coupling constants for the effective interaction. As usual, two of them are chosen to be density dependent:

$$C_t^\rho[\rho_{00}] = A_t^\rho + B_t^\rho \rho_{00}^\alpha(r),$$
$$C_t^s[\rho_{00}] = A_t^s + B_t^s \rho_{00}^\alpha(r). \tag{B3}$$

Here ρ_{t0}, s_{t0}, τ_{t0}, T_{t0}, j_{t0}, $\overset{\leftrightarrow}{J}_{t0}$, and J_{t0} are local densities and currents, which are derived from the general density matrices for protons and neutrons

$$\rho_{00}(r\sigma, r'\sigma') = \rho_n(r\sigma, r'\sigma') + \rho_p(r\sigma, r'\sigma'),$$
$$\rho_{10}(r\sigma, r'\sigma') = \rho_n(r\sigma, r'\sigma') - \rho_p(r\sigma, r'\sigma'), \tag{B4}$$

where

$$\rho_n(r\sigma, r'\sigma') = \sum_{KK',\text{neutron}} \psi_{K'}^*(r'\sigma')\psi_K(r\sigma)\rho_{KK'},$$
$$\rho_p(r\sigma, r'\sigma') = \sum_{KK',\text{proton}} \psi_{K'}^*(r'\sigma')\psi_K(r\sigma)\rho_{KK'}, \tag{B5}$$

and $\sigma = \pm\frac{1}{2}$ labels the spin components so that, for example, $\psi_K(r\sigma)$ is a spin component of the single-particle wave function associated with the state K. Defining

$$\rho_{t0}(r, r') = \sum_{\sigma=\pm} \rho_{t0}(r\sigma, r'\sigma),$$
$$s_{t0}(r, r') = \sum_{\sigma,\sigma'=\pm} \rho_{t0}(r\sigma, r'\sigma')\,\sigma_{\sigma'\sigma}, \tag{B6}$$

where $\sigma_{\sigma'\sigma} = \langle\sigma'|\sigma|\sigma\rangle$ is a matrix element of the vector of Pauli spin matrices, we write the local densities and currents as

$$\rho_{t0}(r) = \rho_{t0}(r, r),$$
$$s_{t0}(r) = s_{t0}(r, r),$$
$$\tau_{t0}(r) = \nabla\cdot\nabla' \rho_{t0}(r, r')|_{r=r'},$$
$$T_{t0}(r) = \nabla\cdot\nabla' s_{t0}(r, r')|_{r=r'}, \tag{B7}$$
$$j_{t0}(r) = -\frac{i}{2}(\nabla - \nabla')\rho_{t0}(r, r')|_{r=r'},$$
$$J_{t0,ij}(r) = -\frac{i}{2}(\nabla - \nabla')_i\, s_{t0,j}(r, r')|_{r=r'},$$

$$\overset{\leftrightarrow}{J}{}_{t0}^2(r) = \sum_{ij=xyz} J_{t0,ij}^2,$$

$$J_{t0}(r) = -\frac{i}{2}(\nabla - \nabla')\times s_{t0}(r, r')|_{r=r'}.$$

The Coulomb energy functional is given by

$$E_{\text{Coul}}[\rho_p] = \frac{e^2}{2}\iint d^3r\, d^3r'\, \frac{\rho_p(r)\rho_p(r')}{|r - r'|}$$

$$- \frac{3}{4}e^2\left(\frac{3}{\pi}\right)^{\frac{1}{3}}\int d^3r\, \rho_p^{4/3}(r), \tag{B8}$$

where we make the usual Slater approximation [84] for the exchange term.

For the pairing functional we take the quite general form

$$E_{\text{pair}}[\rho, \kappa, \kappa^*] = E_{\text{pair}}[\rho, \tilde\rho, \tilde\rho^*] = \int d^3r\, C^{\tilde\rho}[\rho_{00}(r)]$$

$$\times \sum_{\tau=p,n} |\tilde\rho_\tau(r)|^2, \tag{B9}$$

where the density-dependent pairing coupling constant $C^{\tilde\rho}[\rho_{00}(r)]$ is an arbitrary function of $\rho_{00}(r)$. The quantity $\tilde\rho_\tau(r)$ is defined as [66]

$$\tilde\rho_\tau(r) = -i\sum_{\sigma\sigma'=\pm} \kappa_\tau(r\sigma, r\sigma')\sigma_{\sigma\sigma'}^y, \quad \tau = \text{proton or neutron}, \tag{B10}$$

with

$$\kappa_n(r\sigma, r'\sigma') = \sum_{KK',\text{neutron}} \psi_{K'}(r'\sigma')\psi_K(r\sigma)\kappa_{KK'},$$
$$\kappa_p(r\sigma, r'\sigma') = \sum_{KK',\text{proton}} \psi_{K'}(r'\sigma')\psi_K(r\sigma)\kappa_{KK'}, \tag{B11}$$

being the standard pairing tensor in the coordinate representation.

The second derivatives of the energy functional in Eq. (A4), as the equation indicates and as we have already noted, can be written as *unsymmetrized* matrix elements $\bar V_{KLK'L'}^{\text{ph}}$ of an effective interaction between uncoupled pairs of single-particle states. The particle-hole matrix elements take the form

$$\bar V_{KLK'L'}^{\text{ph}} = \langle KL | \bar V_{\text{Skyrme}}^{\text{eff}} + \bar V_{\text{Coul}}^{\text{eff}} + \bar V_{\text{pair}}^{\text{eff ph}} | K'L' \rangle. \tag{B12}$$

The last term contains the pairing rearrangement discussed at the end of the previous Appendix.

The effective Skyrme interaction in Eq. (B12) is given by

$$\bar V_{\text{Skyrme}}^{\text{eff}} = (a_0 + b_0\sigma\cdot\sigma' + c_0\vec\tau\cdot\vec\tau' + d_0\sigma\cdot\sigma'\vec\tau\cdot\vec\tau')$$

$$\times \delta(r - r') + (a_1 + b_1\sigma\cdot\sigma' + c_1\vec\tau\cdot\vec\tau'$$

$$+ d_1\,\sigma\cdot\sigma'\vec\tau\cdot\vec\tau')(k^{\dagger2}\delta(r - r') + \delta(r - r')k^2)$$

$$+ (a_2 + b_2\sigma\cdot\sigma' + c_2\vec\tau\cdot\vec\tau' + d_2\sigma\cdot\sigma'\vec\tau\cdot\vec\tau')$$

$$\times k^\dagger\cdot\delta(r - r')\,k + (a_3 + b_3\,\sigma\cdot\sigma'$$

$$+ c_3\vec\tau\cdot\vec\tau' + d_3\,\sigma\cdot\sigma'\vec\tau\cdot\vec\tau')\rho_{00}^\alpha(r)\delta(r - r')$$

$$+ [e_3\,\rho_{10}(r)(\tau^{(0)} + \tau'^{(0)}) + g_3\,s_{00}(r)\cdot(\sigma + \sigma')$$

$$+ m_3\,s_{10}(r)\cdot(\sigma\tau^{(0)} + \sigma'\tau'^{(0)})]\,\rho_{00}^{\alpha-1}(r)\delta(r - r')$$

$$+ [f_3\,\rho_{10}^2(r) + h_3\,s_{00}^2(r) + n_3\,s_{10}^2(r)]\rho_{00}^{\alpha-2}(r)$$

TABLE III. Definitions of a_i, b_i, c_i, d_i ($i = 0, \ldots, 3$), a_4, and c_4 in Eq. (B13).

i	a_i	b_i	c_i	d_i
0	$2A_0^\rho$	$2A_0^s$	$2A_1^\rho$	$2A_1^s$
1	$\frac{1}{2}(C_0^\tau - 4C_0^{\Delta\rho})$	$\frac{1}{2}(C_0^T - 4C_0^{\Delta s})$	$\frac{1}{2}(C_1^\tau - 4C_1^{\Delta\rho})$	$\frac{1}{2}(C_1^T - 4C_1^{\Delta s})$
2	$3C_0^\tau + 4C_0^{\Delta\rho}$	$3C_0^T + 4C_0^{\Delta s}$	$3C_1^\tau + 4C_1^{\Delta\rho}$	$3C_1^T + 4C_1^{\Delta s}$
3	$B_0^\rho(\alpha + 2)(\alpha + 1)$	$2B_0^s$	$2B_1^\rho$	$2B_1^s$
4	$-2i\,C_0^{\nabla J}$		$-2i\,C_1^{\nabla J}$	

$$\times\,\delta(\boldsymbol{r} - \boldsymbol{r}') + (a_4 + c_4\,\vec{\tau}\cdot\vec{\tau}')(\boldsymbol{\sigma} + \boldsymbol{\sigma}')\cdot\boldsymbol{k}^\dagger$$
$$\times\,\delta(\boldsymbol{r} - \boldsymbol{r}')\boldsymbol{k}, \tag{B13}$$

where $\vec{\tau} = (\tau^{(\pm 1)}, \tau^{(0)})$ is the vector of Pauli matrices in isospin space and

$$\boldsymbol{k} = -\frac{i}{2}(\boldsymbol{\nabla} - \boldsymbol{\nabla}') \text{ acting to the right,}$$
$$\boldsymbol{k}^\dagger = \frac{i}{2}(\boldsymbol{\nabla} - \boldsymbol{\nabla}') \text{ acting to the left.} \tag{B14}$$

The coefficients in Eq. (B13) are defined in Tables III and IV. Equation (B13) contains the usual Skyrme-interaction operators, but the energy functional (B2) does not necessarily correspond to a real (density-dependent) two-body Skyrme interaction because the matrix elements are not antisymmetrized. Compared to the case usually discussed in the literature, the more general functional relaxes relations that would otherwise restrict the spin-isospin structure of the effective interaction in Eq. (B13); see, for example, [17] for a discussion of the increased freedom.

The densities and currents that appear in Eq. (B13) come mostly from rearrangement terms and take the values given by the HFB ground state. The isoscalar and isovector spin densities $s_{t0}(\boldsymbol{r})$ vanish when the HFB ground state is time-reversal invariant or spherical as assumed here. The terms containing them will therefore not appear in the expressions for the matrix elements of the effective interaction for such states given in the following.

The effective Coulomb interaction in Eq. (B12), acting between protons, is given by

$$\bar{V}_{\text{Coul}}^{\text{eff}} = \frac{e^2}{|\boldsymbol{r} - \boldsymbol{r}'|} - \frac{e^2}{3}\left(\frac{3}{\pi}\right)^{\frac{1}{3}}\rho_p^{-2/3}(\boldsymbol{r})\delta(\boldsymbol{r} - \boldsymbol{r}'). \tag{B15}$$

Finally, the ph-type pairing-rearrangement terms in Eq. (B12) come from an effective interaction

$$\bar{V}_{\text{pair}}^{\text{eff ph}} = \frac{d^2C^{\tilde\rho}[\rho_{00}(\boldsymbol{r})]}{d\rho_{00}^2(\boldsymbol{r})}\sum_{\tau = p,n}|\tilde\rho_\tau(\boldsymbol{r})|^2\,\delta(\boldsymbol{r}' - \boldsymbol{r}). \tag{B16}$$

The second derivatives with respect to κ, κ^* also can be written as unsymmetrized matrix elements of effective inter-

actions, this time in the particle-particle channel. The particle-particle effective interaction entering the matrix elements

$$\bar{V}_{KK'LL'}^{\text{pp}} = \langle KK'|\bar{V}_{\text{pair}}^{\text{eff pp}}|LL'\rangle \tag{B17}$$

is obtained from Eq. (B9) through Eq. (A5) as

$$\bar{V}_{\text{pair}}^{\text{eff pp}} = C^{\tilde\rho}[\rho_{00}(\boldsymbol{r})](3 - \boldsymbol{\sigma}\cdot\boldsymbol{\sigma}' - \vec{\tau}\cdot\vec{\tau}' - \boldsymbol{\sigma}\cdot\boldsymbol{\sigma}'\,\vec{\tau}\cdot\vec{\tau}')$$
$$\times\,\delta(\boldsymbol{r} - \boldsymbol{r}'). \tag{B18}$$

In the numerical calculations of this paper, we use a volume pairing-energy functional, that is,

$$C^{\tilde\rho} = \tfrac{1}{2}V_0 = \text{const.} \tag{B19}$$

Last of all are the mixed functional derivatives involving both ρ and κ (or $\tilde\rho$) in Eq. (A6). They also can be written as the unsymmetrized matrix elements of an effective interaction:

$$\bar{V}_{K'KL'L}^{\text{3p1h}} = \langle L'K'|\bar{V}_{\text{pair}}^{\text{eff 3p1h}}|LT(K)\rangle, \tag{B20}$$

where $T(K)$ denotes the time-reversed state of K, and the 3p1h effective interaction itself is

$$\bar{V}_{\text{pair}}^{\text{eff 3p1h}} = \frac{dC^{\tilde\rho}[\rho_{00}(\boldsymbol{r})]}{d\rho_{00}(\boldsymbol{r})}[\tilde\rho_p(\boldsymbol{r})(1 - \tau_z') + \tilde\rho_n(\boldsymbol{r})(1 + \tau_z')]$$
$$\times\,\delta(\boldsymbol{r}' - \boldsymbol{r}), \tag{B21}$$

where τ_z' acts on the single-particle states K' and $T(K)$ in Eq. (B20), and the eigenvalues 1 and -1 are assigned to the neutron and proton, respectively.

2. Calculation of matrix elements

To calculate the coupled matrix elements in Eqs. (A14)–(A16), we use an intermediate LS scheme:

$$\langle[\mu\mu']J_k|\bar{V}|[\nu\nu']J_k\rangle$$
$$= \sum_{LL'S}\hat{j}_\mu\hat{j}_{\mu'}\hat{j}_\nu\hat{j}_{\nu'}\hat{L}\hat{L}'\hat{S}^2\begin{Bmatrix} l_\mu & l_{\mu'} & L \\ 1/2 & 1/2 & S \\ j_\mu & j_{\mu'} & J_k \end{Bmatrix}\begin{Bmatrix} l_\nu & l_{\nu'} & L' \\ 1/2 & 1/2 & S \\ j_\nu & j_{\nu'} & J_k \end{Bmatrix}$$
$$\times\,\langle(l_\mu l_{\mu'})LS; J_k|\bar{V}|(l_\nu l_{\nu'})L'S; J_k\rangle, \tag{B22}$$

$$\hat{j}_\mu \equiv \sqrt{2j_\mu + 1}. \tag{B23}$$

TABLE IV. Definitions of the coefficients appearing in the rearrangement terms in Eq. (B13).

i	e_i	f_i	g_i	h_i	m_i	n_i
3	$2\alpha B_1^\rho$	$\alpha(\alpha - 1)B_1^\rho$	$2\alpha B_0^s$	$\alpha(\alpha - 1)B_0^s$	$2\alpha B_1^s$	$\alpha(\alpha - 1)B_1^s$

Equation (B13) gives
(i) proton-proton or neutron-neutron matrix elements:

$$\langle(l_\mu l_{\mu'})LS; J_k|\bar{V}_{\text{Skyrme}}^{\text{eff}}|(l_\nu l_{\nu'})L'S; J_k\rangle$$

$$= \{a_0 + c_0 + (2S(S+1)-3)(b_0+d_0)\}\langle(l_\mu l_{\mu'})LS; J_k|\delta(\boldsymbol{r}-\boldsymbol{r}')|(l_\nu l_{\nu'})L'S; J_k\rangle$$

$$+ \{a_1 + c_1 + (2S(S+1)-3)(b_1+d_1)\}\langle(l_\mu l_{\mu'})LS; J_k|\boldsymbol{k}^{\dagger 2}\delta(\boldsymbol{r}-\boldsymbol{r}') + \delta(\boldsymbol{r}-\boldsymbol{r}')\boldsymbol{k}^2|(l_\nu l_{\nu'})L'S; J_k\rangle$$

$$+ \{a_2 + c_2 + (2S(S+1)-3)(b_2+d_2)\}\langle(l_\mu l_{\mu'})LS; J_k|\boldsymbol{k}^\dagger \cdot \delta(\boldsymbol{r}-\boldsymbol{r}')\boldsymbol{k}|(l_\nu l_{\nu'})L'S; J_k\rangle$$

$$+ \{a_3 + c_3 + (2S(S+1)-3)(b_3+d_3)\}\langle(l_\mu l_{\mu'})LS; J_k|\rho_{00}^\alpha(\boldsymbol{r})\delta(\boldsymbol{r}-\boldsymbol{r}')|(l_\nu l_{\nu'})L'S; J_k\rangle$$

$$+ 2e_3\langle(l_\mu l_{\mu'})LS; J_k|\rho_{10}(\boldsymbol{r})\rho_{00}^{\alpha-1}(\boldsymbol{r})\delta(\boldsymbol{r}-\boldsymbol{r}')|(l_\nu l_{\nu'})L'S; J_k\rangle \times \begin{cases}(-1), & \text{proton} \\ 1, & \text{neutron}\end{cases}$$

$$+ f_3\langle(l_\mu l_{\mu'})LS; J_k|\rho_{10}^2(\boldsymbol{r})\rho_{00}^{\alpha-2}(\boldsymbol{r})\delta(\boldsymbol{r}-\boldsymbol{r}')|(l_\nu l_{\nu'})L'S; J_k\rangle$$

$$+ (a_4 + c_4)\langle(l_\mu l_{\mu'})LS; J_k|(\boldsymbol{\sigma}+\boldsymbol{\sigma}')\cdot\boldsymbol{k}^\dagger \times \delta(\boldsymbol{r}-\boldsymbol{r}')\boldsymbol{k}|(l_\nu l_{\nu'})L'S; J_k\rangle, \tag{B24}$$

and (ii) proton-neutron matrix elements:

$$\langle(l_\mu l_{\mu'})LS; J_k|\bar{V}_{\text{Skyrme}}^{\text{eff}}|(l_\nu l_{\nu'})L'S; J_k\rangle$$

$$= \{a_0 - c_0 + (2S(S+1)-3)(b_0-d_0)\}\langle(l_\mu l_{\mu'})LS; J_k|\delta(\boldsymbol{r}-\boldsymbol{r}')|(l_\nu l_{\nu'})L'S; J_k\rangle$$

$$+ \{a_1 - c_1 + (2S(S+1)-3)(b_1-d_1)\}\langle(l_\mu l_{\mu'})LS; J_k|\boldsymbol{k}^{\dagger 2}\delta(\boldsymbol{r}-\boldsymbol{r}') + \delta(\boldsymbol{r}-\boldsymbol{r}')\boldsymbol{k}^2|(l_\nu l_{\nu'})L'S; J_k\rangle$$

$$+ \{a_2 - c_2 + (2S(S+1)-3)(b_2-d_2)\}\langle(l_\mu l_{\mu'})LS; J_k|\boldsymbol{k}^\dagger \cdot \delta(\boldsymbol{r}-\boldsymbol{r}')\boldsymbol{k}|(l_\nu l_{\nu'})L'S; J_k\rangle$$

$$+ \{a_3 - c_3 + (2S(S+1)-3)(b_3-d_3)\}\langle(l_\mu l_{\mu'})LS; J_k|\rho_{00}^\alpha(\boldsymbol{r})\delta(\boldsymbol{r}-\boldsymbol{r}')|(l_\nu l_{\nu'})L'S; J_k\rangle$$

$$+ f_3\langle(l_\mu l_{\mu'})LS; J_k|\rho_{10}^2(\boldsymbol{r})\rho_{00}^{\alpha-2}(\boldsymbol{r})\delta(\boldsymbol{r}-\boldsymbol{r}')|(l_\nu l_{\nu'})L'S; J_k\rangle$$

$$+ (a_4 - c_4)\langle(l_\mu l_{\mu'})LS; J_k|(\boldsymbol{\sigma}+\boldsymbol{\sigma}')\cdot\boldsymbol{k}^\dagger \times \delta(\boldsymbol{r}-\boldsymbol{r}')\boldsymbol{k}|(l_\nu l_{\nu'})L'S; J_k\rangle. \tag{B25}$$

We use the canonical (and real) radial wave functions $R_\mu(r)$, the angular wave functions $Y_{l_\mu l_\mu^z}(\Omega)$, and the spin wave functions to write the nontrivial matrix elements included in Eqs. (B24) and (B25) as

$$\langle(l_\mu l_{\mu'})LS; J_k|\delta(\boldsymbol{r}-\boldsymbol{r}')|(l_\nu l_{\nu'})L'S; J_k\rangle$$

$$= \int dr\, r^2 R_\mu(r)R_{\mu'}(r)R_\nu(r)R_{\nu'}(r)\delta_{LL'}\int d\Omega\,\left[Y_{l_\mu}(\Omega)Y_{l_{\mu'}}(\Omega)\right]_{L0}^*$$

$$\times \left[Y_{l_\nu}(\Omega)Y_{l_{\nu'}}(\Omega)\right]_{L0}, \tag{B26}$$

$$\int d\Omega\,\left[Y_{l_\mu}(\Omega)Y_{l_{\mu'}}(\Omega)\right]_{L0}^* \left[Y_{l_\nu}(\Omega)Y_{l_{\nu'}}(\Omega)\right]_{L0}$$

$$= \frac{1}{4\pi}\hat{l}_\mu\hat{l}_{\mu'}\hat{l}_\nu\hat{l}_{\nu'}\begin{pmatrix}l_\mu & l_{\mu'} & L \\ 0 & 0 & 0\end{pmatrix}\begin{pmatrix}l_\nu & l_{\nu'} & L \\ 0 & 0 & 0\end{pmatrix}, \tag{B27}$$

$$\langle(l_\mu l_{\mu'})LS; J_k|\delta(\boldsymbol{r}-\boldsymbol{r}')\boldsymbol{k}^2|(l_\nu l_{\nu'})L'S; J_k\rangle$$

$$= -\frac{1}{4}\delta_{LL'}\int d\Omega\,\left[Y_{l_\mu}(\Omega)Y_{l_{\mu'}}(\Omega)\right]_{L0}^*\left[Y_{l_\nu}(\Omega)Y_{l_{\nu'}}(\Omega)\right]_{L0}$$

$$\times \int dr\, r^2 R_\mu(r)R_{\mu'}(r)\left\{\left[\left(\frac{d^2}{dr^2}+\frac{2}{r}\frac{d}{dr}-\frac{l_\nu(l_\nu+1)}{r^2}\right)\right.\right.$$

$$\times R_\nu(r)\bigg]R_{\nu'}(r) + R_\nu(r)\left[\left(\frac{d^2}{dr^2}+\frac{2}{r}\frac{d}{dr}-\frac{l_{\nu'}(l_{\nu'}+1)}{r^2}\right)\right.$$

$$\times R_{\nu'}(r)\bigg]\bigg\} - \sum_{\Delta l_\nu=0,1}\sum_{\Delta l_{\nu'}=0,1}\frac{1}{2}\sqrt{(l_\nu+\Delta l_\nu)(l_{\nu'}+\Delta l_{\nu'})}$$

$$\times \begin{Bmatrix}l_{\nu'}-1+2\Delta l_{\nu'} & l_\nu-1+2\Delta l_\nu & L \\ l_\nu & l_{\nu'} & 1\end{Bmatrix}\int dr\, r^2 R_\mu(r)$$

$$\times R_{\mu'}(r)\left\{(l_\nu+1-\Delta l_\nu)\frac{R_\nu(r)}{r}+(-)^{\Delta l_\nu}\frac{dR_\nu(r)}{dr}\right\}$$

$$\times \left\{(l_{\nu'}+1-\Delta l_{\nu'})\frac{R_{\nu'}(r)}{r}+(-)^{\Delta l_{\nu'}}\frac{dR_{\nu'}(r)}{dr}\right\}$$

$$\times \delta_{LL'}\int d\Omega\,\left[Y_{l_\mu}(\Omega)Y_{l_{\mu'}}(\Omega)\right]_{L0}^*$$

$$\times \left[Y_{l_{\nu'}-1+2\Delta l_{\nu'}}(\Omega)Y_{l_\nu-1+2\Delta l_\nu}(\Omega)\right]_{L0}, \tag{B28}$$

$$\langle(l_\mu l_{\mu'})LS; J_k|\boldsymbol{k}^\dagger \cdot \delta(\boldsymbol{r}-\boldsymbol{r}')\boldsymbol{k}|(l_\nu l_{\nu'})L'S; J_k\rangle$$

$$= -\frac{\sqrt{3}}{\hat{L}}\delta_{LL'}\langle(l_\mu l_{\mu'})L||(\boldsymbol{k}^\dagger \cdot \delta(\boldsymbol{r}-\boldsymbol{r}')\boldsymbol{k})_0||(l_\nu l_{\nu'})L\rangle, \tag{B29}$$

$$\langle(l_\mu l_{\mu'})LS; J_k|i(\boldsymbol{\sigma}+\boldsymbol{\sigma}')\cdot\boldsymbol{k}^\dagger \times \delta(\boldsymbol{r}-\boldsymbol{r}')\boldsymbol{k}|(l_\nu l_{\nu'})L'S; J_k\rangle$$

$$= (-)^{1+L'+J_k}4\sqrt{3}\langle(l_\mu l_{\mu'})L||(\boldsymbol{k}^\dagger \cdot \delta(\boldsymbol{r}-\boldsymbol{r}')\boldsymbol{k})_1||(l_\nu l_{\nu'})L'\rangle$$

$$\times \begin{Bmatrix}1 & L' & J_k \\ L & 1 & 1\end{Bmatrix}\delta_{S1}. \tag{B30}$$

The square brackets around products of spherical harmonics and the parentheses surrounding products of operators indicate angular-momentum coupling.

To evaluate Eqs. (B29) and (B30), one can use

$$\langle(l_\mu l_{\mu'})L||(\boldsymbol{k}^\dagger \cdot \delta(\boldsymbol{r}-\boldsymbol{r}')\boldsymbol{k})_I||(l_\nu l_{\nu'})L'\rangle$$

$$= \left[\frac{1}{4}\sum_{\Delta l_\mu=0,1}\sum_{\Delta l_\nu=0,1}\sum_{l_{\mu\mu'}}\int dr r^2 \left\{(l_\mu+1-\Delta l_\mu)\frac{R_\mu(r)}{r}\right.\right.$$

$$
\begin{aligned}
&+ (-)^{\Delta l_\mu} \frac{d R_\mu(r)}{dr} \Bigg\} R_{\mu'}(r) \Bigg\{ (l_\nu + 1 - \Delta l_\nu) \frac{R_\nu(r)}{r} \\
&+ (-)^{\Delta l_\nu} \frac{d R_\nu(r)}{dr} \Bigg\} R_{\nu'}(r) \sqrt{l_\mu + \Delta l_\mu} \sqrt{l_\nu + \Delta l_\nu} \\
&\times \sqrt{2l_\mu + 4\Delta l_\mu - 1}\, \hat{l}_{\mu'} \sqrt{2l_\nu + 4\Delta l_\nu - 1}\, \hat{l}_{\nu'} \\
&\times \frac{1}{4\pi} \hat{l}^2_{\mu\mu'} \hat{L} \hat{L}' \hat{I} (-)^{l_\mu + l_{\mu'} + L + I + 1}
\begin{Bmatrix} I & L' & L \\ l_{\mu\mu'} & 1 & 1 \end{Bmatrix} \\
&\times \begin{Bmatrix} l_{\mu\mu'} & L & 1 \\ l_\mu & l_\mu + 2\Delta l_\mu - 1 & l_{\mu'} \end{Bmatrix}
\begin{Bmatrix} l_{\mu\mu'} & L' & 1 \\ l_\nu & l_\nu + 2\Delta l_\nu - 1 & l_{\nu'} \end{Bmatrix} \\
&\times \begin{pmatrix} l_\mu + 2\Delta l_\mu - 1 & l_{\mu'} & l_{\mu\mu'} \\ 0 & 0 & 0 \end{pmatrix}
\begin{pmatrix} l_\nu + 2\Delta l_\nu - 1 & l_{\nu'} & l_{\mu\mu'} \\ 0 & 0 & 0 \end{pmatrix} \Bigg] \\
&- (-)^{l_\nu + l_{\nu'} + L'} [\nu \leftrightarrow \nu'] - (-)^{l_\mu + l_{\mu'} + L} [\mu \leftrightarrow \mu'] \\
&+ [\mu \leftrightarrow \mu' \text{ and } \nu \leftrightarrow \nu'],
\end{aligned} \tag{B31}
$$

where for reduced matrix elements we have used the convention

$$
\langle LL_z | \hat{O}_{lm} | L' L'_z \rangle = \frac{1}{\hat{L}} \langle L' L'_z lm | L L_z \rangle \langle L || \hat{O}_l || L' \rangle \tag{B32}
$$

and made the abbreviation

$$
\begin{aligned}
&[A_{\mu\mu'\nu\nu'}] - (-)^{l_\nu + l_{\nu'} + L'} [\nu \leftrightarrow \nu'] - (-)^{l_\mu + l_{\mu'} + L} \\
&\quad \times [\mu \leftrightarrow \mu'] + [\mu \leftrightarrow \mu' \text{ and } \nu \leftrightarrow \nu'] \\
&\equiv A_{\mu\mu'\nu\nu'} - (-)^{l_\nu + l_{\nu'} + L'} A_{\mu\mu'\nu'\nu} \\
&\quad - (-)^{l_\mu + l_{\mu'} + L} A_{\mu'\mu\nu\nu'} + A_{\mu'\mu\nu'\nu}.
\end{aligned} \tag{B33}
$$

Equation (B26), modified to include additional factors in the radial integral, can also be used (together with the subsequent equations) to evaluate the matrix elements of the terms involving $\rho_{00}^\alpha(\mathbf{r})$ in $\bar{V}_{\text{Skyrme}}^{\text{eff}}$, the Coulomb-exchange interaction, and the contributions of the pairing functional to the effective ph, pp, and 3p1h interactions. The Coulomb-direct term can be evaluated in a similar but slightly more complicated way, via a multipole expansion.

In the main part of this paper we used the Skyrme functional SkM*, which is usually parametrized as in interaction in terms of coefficients t_0, t_1, t_2, t_3, x_0, x_1, x_2, x_3, and W_0. The relations between these coefficients and those used here, if no terms are neglected, are [65,82]

$$
\begin{aligned}
C_0^\rho &= \tfrac{3}{8} t_0 + \tfrac{3}{48} t_3 \, \rho_{00}^\alpha, & C_1^\rho &= -\tfrac{1}{4} t_0 \left(\tfrac{1}{2} + x_0 \right) - \tfrac{1}{24} t_3 \left(\tfrac{1}{2} + x_3 \right) \rho_{00}^\alpha, \\
C_0^s &= -\tfrac{1}{4} t_0 \left(\tfrac{1}{2} - x_0 \right) - \tfrac{1}{24} t_3 \left(\tfrac{1}{2} - x_3 \right) \rho_{00}^\alpha, & C_1^s &= -\tfrac{1}{8} t_0 - \tfrac{1}{48} t_3 \, \rho_{00}^\alpha, \\
C_0^\tau &= \tfrac{3}{16} t_1 + \tfrac{1}{4} t_2 \left(\tfrac{5}{4} + x_2 \right), & C_1^\tau &= -\tfrac{1}{8} t_1 \left(\tfrac{1}{2} + x_1 \right) + \tfrac{1}{8} t_2 \left(\tfrac{1}{2} + x_2 \right), \\
C_0^T &= -\tfrac{1}{8} t_1 \left(\tfrac{1}{2} - x_1 \right) + \tfrac{1}{8} t_2 \left(\tfrac{1}{2} + x_2 \right), & C_1^T &= -\tfrac{1}{16} t_1 + \tfrac{1}{16} t_2, \\
C_0^{\Delta\rho} &= -\tfrac{9}{64} t_1 + \tfrac{1}{16} t_2 \left(\tfrac{5}{4} + x_2 \right), & C_1^{\Delta\rho} &= \tfrac{3}{32} t_1 \left(\tfrac{1}{2} + x_1 \right) + \tfrac{1}{32} t_2 \left(\tfrac{1}{2} + x_2 \right), \\
C_0^{\Delta s} &= \tfrac{3}{32} t_1 \left(\tfrac{1}{2} - x_1 \right) + \tfrac{1}{32} t_2 \left(\tfrac{1}{2} + x_2 \right), & C_1^{\Delta s} &= \tfrac{3}{64} t_1 + \tfrac{1}{64} t_2, \\
C_0^{\nabla J} &= -\tfrac{3}{4} W_0, & C_1^{\nabla J} &= -\tfrac{1}{4} W_0.
\end{aligned} \tag{B34}
$$

In the HF fits that originally determined the SkM* parameters, the effects of C_t^T (the "J^2 terms") were neglected because of technical difficulties. These terms have often been included in subsequent RPA calculations. To maintain self-consistency here, we have set them to zero both in the HFB calculation and in the QRPA.

[1] 2002 NSAC Long-Range Plan (LRP_5547_FINAL.pdf), http://www.sc.doe.gov/henp/np/nsac.

[2] 2004 NUPECC Long-Range Plan (long_range_plan_2004.pdf), http://www.nupecc.org/lrp02.

[3] J. Carlson, B. Holstein, X. Ji, G. McLaughlin, B. Müller, W. Nazarewicz, K. Rajagopal, W. Roberts, and X.-N. Wang, arXiv:nucl-th/0311056.

[4] J. Dobaczewski and W. Nazarewicz, Philos. Trans. R. Soc. London Ser. A **356**, 2007 (1998).

[5] S. Goriely, M. Samyn, P.-H. Heenen, J. Pearson, and F. Tondeur, Phys. Rev. C **66**, 024326 (2002).

[6] S. Goriely, M. Samyn, M. Bender, and J. Pearson, Phys. Rev. C **68**, 054325 (2003).

[7] M. Stoitsov, J. Dobaczewski, W. Nazarewicz, S. Pittel, and D. Dean, Phys. Rev. C **68**, 054312 (2003).

[8] P. Ring and P. Schuck, *The Nuclear Many-Body Problem* (Springer-Verlag, Berlin, 1980).

[9] S. Shlomo and A. Sanzhur, Phys. Rev. C **65**, 044310 (2002).

[10] B. Agrawal, S. Shlomo, and A. Sanzhur, Phys. Rev. C **67**, 034314 (2003).

[11] B. Agrawal and S. Shlomo, Phys. Rev. C. **70**, 014308 (2004).

[12] M. Tohyama and P. Schuck, Eur. Phys. J. A **19**, 203 (2004).

[13] D. Rowe, *Nuclear Collective Motion, Models and Theory* (Methuen, London, 1970).

[14] M. Waroquier, J. Ryckebusch, J. Moreau, K. Heyde, N. Blasi, and S. van der Werf, Phys. Rep. **148**, 249 (1987).

[15] G. Colò, P. Bortignon, D. Sarchi, D. Khoa, E. Khan, and N. V. Giai, Nucl. Phys. **A722**, 111c (2003).

[16] J. Engel, M. Bender, J. Dobaczewski, W. Nazarewicz, and R. Surman, Phys. Rev. C **60**, 14302 (1999).

[17] M. Bender, J. Dobaczewski, J. Engel, and W. Nazarewicz, Phys. Rev. C **65**, 054322 (2002).

[18] G. Giambrone, S. Scheit, F. Barranco, P. Bortignon, G. Colò, D. Sarchi, and E. Vigezzi, Nucl. Phys. **A726**, 3 (2003).

[19] S. Shlomo and G. Bertsch, Nucl. Phys. **A243**, 507 (1975).

[20] K. Liu and N. V. Giai, Phys. Lett. **B65**, 23 (1976).

[21] J. B. Touv, A. Moalem, and S. Shlomo, Nucl. Phys. **A339**, 303 (1980).

[22] I. Hamamoto, H. Sagawa, and X. Zhang, Phys. Rev. C **55**, 2361 (1997).

[23] I. Hamamoto, H. Sagawa, and X. Zhang, Phys. Rev. C **57**, 1064(R) (1998).

[24] I. Hamamoto and H. Sagawa, Phys. Rev. C **60**, 064314 (1999).

[25] I. Hamamoto and H. Sagawa, Phys. Rev. C **62**, 024319 (2000).

[26] A. Kolomiets, O. Pochivalov, and S. Shlomo, Phys. Rev. C **61**, 034312 (2000).

[27] H. Sagawa, Phys. Rev. C **65**, 064314 (2002).

[28] I. Hamamoto and H. Sagawa, Phys. Rev. C **66**, 044315 (2002).

[29] S. Shlomo and B. Agrawal, Nucl. Phys. **A722**, 98c (2003).

[30] K. Hagino and H. Sagawa, Nucl. Phys. **A695**, 82 (2001).

[31] M. Matsuo, Nucl. Phys. **A696**, 371 (2001).

[32] M. Matsuo, Prog. Theor. Phys. Suppl. **146**, 110 (2002).

[33] E. Khan, N. Sandulescu, M. Grasso, and N. V. Giai, Phys. Rev. C **66**, 024309 (2002).

[34] E. Khan, N. Sandulescu, N. V. Giai, and M. Grasso, Phys. Rev. C **69**, 014314 (2004).

[35] M. Yamagami and N. V. Giai, Phys. Rev. C **69**, 034301 (2004).

[36] S. Goriely and E. Khan, Nucl. Phys. **A706**, 217 (2002).

[37] S. Goriely, E. Khan, and M. Samyn, Nucl. Phys. **A739**, 331 (2004).

[38] A. Platonov and E. Saperstein, Nucl. Phys. **A486**, 63 (1988).

[39] S. Kamerdzhiev, J. Speth, and G. Tertychny, Phys. Rep. **393**, 1 (2004).

[40] S. Fayans, A. Platonov, G. Graw, and D. Hofer, Nucl. Phys. **A577**, 557 (1994).

[41] D. Horen, G. Satchler, S. Fayans, and E. Trykov, Nucl. Phys. **A600**, 193 (1996).

[42] I. Borzov, A. Fayans, and E. Trykov, Nucl. Phys. **A584**, 335 (1995).

[43] I. Borzov, A. Fayans, E. Krömer, and D. Zawischa, Z. Phys. A **355**, 117 (1996).

[44] S. Kamerdzhiev, R. Liotta, E. Litvinova, and V. Tselyaev, Phys. Rev. C **58**, 172 (1998).

[45] S. Kamerdzhiev, E. V. Litvinova, and D. Zawischa, Eur. Phys. J. A **12**, 285 (2001).

[46] I. Borzov, Phys. Rev. C **67**, 025802 (2003).

[47] S. Kamerdzhiev and E. V. Litvinova, Phys. At. Nucl. **67**, 183 (2004).

[48] P. Ring, Z. Ma, N. V. Giai, D. Vretenar, A. Wandelt, and L. Cao, Nucl. Phys. **A694**, 249 (2001).

[49] D. Vretenar, N. Paar, P. Ring, and G. Lalazissis, Phys. Rev. C **63**, 047301 (2001).

[50] Z. Ma, A. Wandelt, N. V. Giai, D. Vretenar, P. Ring, and L. Cao, Nucl. Phys. **A703**, 222 (2002).

[51] D. Vretenar, N. Paar, P. Ring, and T. Nikšić, Phys. Rev. C **65**, 021301 (2002).

[52] T. Nikšić, D. Vretenar, and P. Ring, Phys. Rev. C **66**, 064302 (2002).

[53] Z. Ma, L. Cao, N. V. Giai, and P. Ring, Nucl. Phys. **A722**, 491c (2003).

[54] D. Vretenar, T. Nikšić, N. Paar, and P. Ring, Nucl. Phys. **A731**, 281 (2004).

[55] N. Paar, P. Ring, T. Nikšić, and D. Vretenar, Phys. Rev. C **67**, 034312 (2003).

[56] N. Paar, T. Nikšić, D. Vretenar, and P. Ring, Phys. Rev. C **69**, 054303 (2004).

[57] T. Nakatsukasa and K. Yabana, Prog. Theor. Phys. Suppl. **146**, 447 (2002).

[58] T. Nakatsukasa and K. Yabana, Eur. Phys. J. A **20**, 163 (2004).

[59] T. Inakura, M. Yamagami, K. Matsuyanagi, S. Mizutori, H. Imagawa, and Y. Hashimoto, Int. J. Mod. Phys. E **13**, 157 (2004).

[60] H. Imagawa and Y. Hashimoto, Phys. Rev. C **67**, 037302 (2003).

[61] K. Hagino, N. V. Giai, and H. Sagawa, Nucl. Phys. **A731**, 264 (2004).

[62] J. Dobaczewski, W. Nazarewicz, T. Werner, J. Berger, C. Chinn, and J. Dechargé, Phys. Rev. C **53**, 2809 (1996).

[63] P. Ring, N. Paar, T. Nikšić, and D. Vretenar, Nucl. Phys. **A68**, 372 (2003).

[64] J. Engel, G. McLaughlin, and C. Volpe, Phys. Rev. D **67**, 013005 (2003).

[65] E. Perlińka, S. Rohoziski, J. Dobaczewski, and W. Nazarewicz, Phys. Rev. C **69**, 014316 (2004).

[66] J. Dobaczewski, H. Flocard, and J. Treiner, Nucl. Phys. **A422**, 103 (1984).

[67] J. Dobaczewski, W. Nazarewicz, and P.-G. Reinhard, Nucl. Phys. **A693**, 361 (2001).

[68] K. Bennaceur and J. Dobaczewski (to be submitted to Comput. Phys. Commun.).

[69] J. Terasaki, J. Engel, W. Nazarewicz, and M. Stoitsov, Phys. Rev. C **66**, 054313 (2002).

[70] J. Dobaczewski, P. Borycki, W. Nazarewicz, and M. Stoitsov (to be published).

[71] S. Shlomo, V. Kolomietz, and H. Dejbakhsh, Phys. Rev. C **55**, 1972 (1997).

[72] J. Bartel, P. Quentin, M. Brack, C. Guet, and H.-B. Håkansson, Nucl. Phys. **A386**, 79 (1982).

[73] J. Dobaczewski, W. Nazarewicz, and M. Stoitsov, in *The Nuclear Many-Body Problem 2001*, edited by W. Nazarewicz and D. Vretenar (Kluwer, Dordrecht, 2002), p. 181.

[74] J. Dobaczewski, M. Stoitsov, and W. Nazarewicz, arXiv:nucl-th/0404077.

[75] N. Tajima, Phys. Rev. C **69**, 034305 (2004).

[76] J. Blaizot and G. Ripka, *Quantum Theory of Finite Systems* (MIT Press, Cambridge, MA, 1986).

[77] M. Harakeh and A. van der Woude, *Giant Resonances, Fundamental High-Frequency Modes of Nuclear Excitation* (Clarendon Press, Oxford, 2001).

[78] J. Terasaki *et al.* (in preparation).

[79] F. Catara, E. Lanza, M. Nagarajan, and A. Vitturi, Nucl. Phys. **A624**, 449 (1997).

[80] H. Sagawa and H. Esbensen, Nucl. Phys. **A693**, 448 (2001).

[81] S. Raman, J. C. W. Nestor, and P. Tikkanen, At. Data Nucl. Data Tables **78**, 1 (2001).

[82] J. Dobaczewski and J. Dudek, Phys. Rev. C **52**, 1827 (1995); **55**, 3177(E) (1997).

[83] M. Bender, P.-H. Heenen, and P.-G. Reinhard, Rev. Mod. Phys. **75**, 121 (2003).

[84] J. Slater, Phys. Rev. **81**, 385 (1951).